EIC Detector R&D Progress Report

The EIC Tracking and PID Consortium
(eRD6 Consortium)

January 3, 2020

The eRD6 Consortium

Project ID: eRD6

Project Name: Tracking & PID detector R&D towards an EIC detector

Period Reported: from July 2019 to December 2019

Brookhaven National Lab (BNL): Craig Woody

Florida Institute of Technology (Fl. Tech): Marcus Hohlmann

INFN Trieste: Silvia Dalla Torre

Stony Brook University (SBU): Klaus Dehmelt, Thomas Hemmick

Temple University (TU): Matt Posik, Amilkar Quintero, Bernd Surrow

University of Virginia (UVa): Kondo Gnanvo, Nilanga Liyanage

Yale University: Richard Majka, Nikolai Smirnov

Project Members:

BNL: B. Azmoun, A. Kiselev, J. Kuczewski, M. L. Purschke, C. Woody

BNL - Medium Energy Group: E. C. Aschenauer

Fl. Tech: M. Bomberger, J. Collins, M. Hohlmann

INFN Trieste: S. Dalla Torre, S. Levorato, F. Tessarotto

SBU: K. Dehmelt, A. Deshpande, P. Garg, T. K. Hemmick, A. Kulkarni, C. Perez Lara, V. Zakharov

TU: M. Posik, A. Quintero, B. Surrow

UVa: K. Gnanvo, N. Liyanage, Minh Dao, John Boyd, Huong Nguyen

Yale University: R. Majka, N. Smirnov

Contact Person: Kondo Gnanvo; kgnanvo@virginia.edu

Contents

1 Brief overview of project histories and the document structure

The overall main focus of the R&D conducted by the eRD6 consortium has been the development of micro-pattern gas detectors (MPGD's) for tracking and particle identification at a future EIC. Some particular emphasis has been given to applying GEM technology in this context. While each institution has been focusing on certain technical aspects, much synergy has been produced with several collaborative efforts created over the years. For central tracking, BNL, Stony Brook, and Yale have been mounting a long-term investigation of GEM-based TPCs, while more recently Florida Tech, Temple U., and U. Virginia have teamed up to study the potential for a fast central tracker based on μRWELLs with support also from BNL. The latter three groups have previously also closely collaborated on the design, production, and testing of large GEM detector for the forward tracker. They jointly designed GEM foils for forward tracker prototypes that could be used by each group and they have conducted beam tests together at Fermilab. The PID effort was spearheaded and is continued by Stony Brook with a focus on optical elements, which more recently is being complemented by the INFN Trieste efforts on MPGD-based photon detection. The entire group meets bi-weekly to discuss progress and problems and to coordinate efforts. In addition, a smaller subgroup meets regularly on simulation efforts.

Following the recommendation from the review committee in its Jan 2019 report, we have organized the structure of this research report to better reflect this internal collaboration within our consortium. Instead of each group reporting all their findings, concerns, and plans separately, we organize the report by technical topic with each institution reporting its contribution to each topic in the corresponding section. We hope that this will present a more cohesive picture of the overall joint R&D activities of our consortium.

1.1 Brookhaven National Lab (BNL)

The group at BNL is mainly engaged in optimizing micro-pattern gaseous detectors (MPGD's) for reading out a time projection chamber (TPC) for use at the EIC.

Over the last few years we have built and tested numerous planar GEM detectors with long (˜16mm) and short (˜3mm) drift regions and have equipped them with both zigzag pad and strip readout geometries in an effort to study the spatial and angular resolution of a host of detector configurations. The results of these efforts were published in a peer reviewed journal in 2014 [1].

In addition, in collaboration with Stony Brook U. and Yale U., we have built a prototype combination TPC-Cherenkov (TPCC) detector to study the feasibility of performing tracking and pID measurements in a common detector volume. The results from these tests were positive and are detailed in a paper recently published in the peer review journal, IEEE TNS [2].

More recently we have focused on optimizing the design of the readout plane for a GEM detector made of zigzag shaped charge collecting anodes. We performed both simulations and test beam measurements to study which geometrical parameters of the zigzag shape drive the performance of the readout. The results of these investigations were published in a peer review journal [3], with collaborators from Florida Tech and Stony Brook U and a more recent paper on this topic [4] was submitted for publication to IEEE TNS.

Our focus is now primarily on investigating various avalanche technologies for a TPC readout including GEMs, Micromegas, a combination of the two, and μRWELL. This includes finding optimal zigzag parameter sets for the readout of each avalanche scheme, which can be very different than what was studied in the past. It must be noted, however, that the effort to further optimize zigzag readout patterns in general is not covered under the purview of this R&D program, but rather under a separate BNL funded LDRD grant. Nonetheless, we will briefly report on the zigzag R&D since the readout is a fundamental aspect of the detector.

1.2 Florida Institute of Technology (Florida Tech)

The Florida Tech group initially focused on the development of large low-mass GEM detectors with low channel count for the forward tracker (FT) of the EIC detector. In the last funding cycle the group begun shifting focus towards R&D on cylindrical μRWELL detectors for a fast central tracker at an EIC detector.

We designed and implemented radial zigzag strips on large readout PCBs to achieve low-channel count while maintaining good spatial resolution. We constructed a first one-meter-long prototype with such a readout at Florida Tech using a purely mechanical construction technique without any gluing and tested it in beams at Fermilab in 2013. This study showed a non-linearity in the position measurement of hits[5]. We subsequently tested small PCBs and a flex-foil with the improved zigzag strip design with highly collimated X-rays at BNL. A substantial reduction in the non-linearity and an improvement in spatial resolution were observed[6].

Next, we designed a second large Triple-GEM detector that implements the drift electrode and a readout electrode with radial zigzag strips on polyimide foils rather than on PCBs to reduce the material in the active detector area[7]. To provide rigidity to this new detector while maintaining low mass, we produced the main support frames from carbon fiber material. We designed the GEM foils for this second detector so that they could also be used for the second UVa FT prototype ("common GEM foil design"). Initial assembly of this second prototype showed that 3D-printed pull-out and frame components made from ABS did not have sufficient material strength to sustain the mechanical forces needed for stretching. They were consequently replaced by stronger PEEK components and the detector was reassembled from scratch. We also added a small simulation component to the forward tracker work.

For the cylindrical μRWELL, we produced a first conceptual hardware design for a full-size cylindrical μRWELL tracker based on a purely mechanical detector assembly technique, which is currently being developed further.

1.3 INFN Trieste (INFN)

The task of the INFN participants to the eRD6 Consortium is "Further development of hybrid MPGDs for single photon detection synergistic to TPC read-out sensors".

Particle identification of electrons and hadrons over a wide momentum range is a key ingredient for the physics programme at EIC. One of the most challenging aspects is hadron identification at high momenta, namely above 6-8 GeV/c, where the only possibility is the use of Cherenkov imaging techniques making use of gaseous radiator. The overall constrains of the experimental set-ups at a collider impose a limited RICH detector length and to operate in magnetic fringing field. The use, for this RICH, of gaseous photon detectors is one of the most likely choice. The goal of our project is an R&D to further develop MPGD-based single photon detectors in order to establish one of the key components of the RICH for high momentum hadrons. This R&D has also some aspects synergistic to the development of TPC sensors: the miniaturization of the read-out elements and the reduction of the Ions Back-Flow (IBF).

The starting point are the hybrid MPGD detectors of single photons [8], developed for the upgrade of the gaseous RICH counter [9, 10, 11, 12] of the COMPASS experiment [13, 14] at CERN SPS. They consists in three multiplication stages: two THick GEMs (THGEM) layers, the first one coated with a CsI film and acting as photocathode, followed by a resistive MicroMegas (MM) multiplication stage. The anode plane is segmented in pads with size 8×8 mm^2. The resistive MM has an original implementation: it is by discrete elements, namely a resistor in series with each pad. The COMPASS photon detectors can operate at gains of at least 3×10^4 and exhibit an IBF rate lower at the 3% level.

The present R&D project develops over several years and it includes further improvements of the hybrid MPGD-based photon detectors in order to match the requirements of high momenta hadron identification at EIC and initial tests relative to the application in gaseous detectors of a novel photocathode concept, based on NanoDiamond (ND) particles [15].

1.4 Stony Brook University (SBU)

SBU is concentrating on the study of Ion Backflow (IBF) for a TPC, a possible candidate for the central tracker in at least one of the detectors for an EIC. Furthermore, the TPC for sPHENIX has the same physical size when used in, e.g., the BeAST EIC detector.

IBF will pose a problem in an EIC detector and the ultimate EIC TPC device must do more than sPHENIX to achieve the same level of position distortion. We are investigating investigate new structures in and around the multiplication stage that promise significant better performance when considering IBF.

The installation of an upgrade to the evaporator used for previous CsI-evaporation has been finalized and is foreseen to produce high quality large size mirrors for RICH applications as well as other applications.

SBU has furthermore proposed to investigate the feasibility of meta-materials for extending the performance of Cherenkov imaging detectors.

1.5 University of Virginia (UVa)

The initial R&D focus of UVa group was on the development of high performance, low mass GEM detector for the forward tracker of an EIC detector. In the last cycle, our focus has shifted towards the development of cylindrical μRWELL technologies for the fast tracker in the central region of an EIC detector.

Two large GEM prototypes with high granularity two-dimensional (2D) U-V strip readout were designed, built and successfully tested at the Fermilab Test Beam Facility (FTBF) in 2013 and 2018. The excellent spatial resolution in both radial and azimuthal direction have been demonstrated for the two prototypes and results of the first prototype were published in [16]. The analysis is ongoing for the second prototype with improved U-V strip readout design for better spatial resolution in both directions.

Though UVa group mainly concentrated on the development of fine structure 2D U-V strip readout, our R&D effort had strong synergies with the ongoing activities with Florida Tech and Temple U. groups. The second UVa large prototype was the fruit of a collaborative effort by the three institutes to develop a "Common EIC GEM foil" to be used in the assembly of three large GEM prototypes (one per institute), each prototype built with a different readout structure and assembly technique. In addition, we are characterizing thin layer chromium GEM (Cr-GEM) foils that, we anticipate, could be used in low mass GEM detectors.

More recently, our R&D effort has shifted towards the characterization of a small planar 2D strip μRWELL prototype as pre-R&D for the fast signal cylindrical μRWELL detector in the central region of EIC detector. We report here, the preliminary results of the extensive and detailed characterization of the prototype.

1.6 Temple University (TU)

Temple University's (TU) initial R&D efforts have been centered around the assembly and characterization of triple-GEM detectors which include commercialized 2D readout, HV, and single-mask GEM foils. The focus of the eRD3 program was a joint R&D effort between TU and the company Tech-Etch, with the ultimate goal of Tech-Etch manufacturing commercially available large area 2D readout, HV, and single-mask GEM foils. This effort also lead to the highly successful large area CCD scanner, which was built to assess the overall geometric properties of the GEM foils as they were produced by Tech-Etch. The GEM CCD scanner has since provided service to the larger MPGD community such as scanning UVa's chromium GEMs, the BoNuS experiment's GEMs, and $\sim$ 1 m long GEMs for the company Mecro. TU is still supporting and maintaining the GEM scanner and its services are available for use.

TU is working closely with FIT and UVa to develop a cylindrical μRWELL central detector which operates in a μTPC mode. TU has thus far been focusing on the simulation of the detector within the EicRoot framework. Our simulation allows one to easily adjust detector properties and responses. Using measurements from

INFN's μRWELL μTPC prototype [17]) we have begun to investigate the momentum resolution and compare its performance to that of a TPC, based on the sPHENIX TPC. However, the μRWELL detector response still needs to be made more realistic and would greatly benefit from data acquired from a μRWELL detector operating as a μTPC. These measurements could then be fed into the simulation.

2 Tracking

2.1 Central Tracker

In its Jan 2019 report, the review committee stated that *"the collaboration is encouraged to continue developing the TPC readout with different electronics and studying the Micromegas and μRWELL with zigzag readout in a planar detector configuration"* and that *"further studies of a cylindrical μRWELL barrel layer to act as a fast-tracking layer in a non-TPC EIC detector are strongly encouraged."* The committee also recommended that *"(the μRWELL) efforts between the various institutions should be coordinated."* We have been following these recommendations closely with respect to the technical developments as detailed below. We have also continued to coordinate the μRWELL efforts with Fl. Tech focusing on the conceptual design of a barrel tracker with cylindrical μRWELLs following guidance from simulation work that the Temple group is currently focusing on. Temple in turn has incorporated measurements from the INFN μRWELL μTPC prototype into the simulation. Meanwhile, UVa has been making strides on the hardware and successfully tested a planar 10 cm $\times$ 10 cm μRWELL detector and sharing their experience with the other groups.

2.1.1 What was planned for this period?

2.1.1.1 TPC studies at Brookhaven National Lab

The goals for the last funding cycle are listed below:

1. Re-install the 4-layer cosmic ray telescope (after it was borrowed for a beam test at Fermilab) and prepare it for studying particle tracks in the prototype TPC, which is installed on the "cosmic ray stand" in the lab.
2. Study track reconstruction in the TPC prototype using various front end electronics (i.e., SAMPA and DREAM).
3. Design and production of a new readout PCB for the prototype TPC. The PCB will consist of a single-zigzag pattern covering the entire readout plane and the pattern will be optimized using beam test data from Fermilab.
4. Start work on implementing a laser beam to simulate tracks in the TPC volume to compliment measurements with cosmic rays.
5. Complete assembly of the high intensity, narrow beam x-ray scanner setup.

2.1.1.2 TPC studies at Stony Brook

The investigation of IBF blocking structures to be used in MPGD-based readout structures for a TPC is ongoing and plans were in particular, to investigate the concept of a passive gating grid.

2.1.1.3 Cylindrical μRWELL studies at Florida Tech

We planned to commission the $10\times10\,\mathrm{cm}^2$ μRWELL prototype with zigzag-strip readout and to characterize its performance using X-rays. We also planned to begin the design of the first prototype for a cylindrical μRWELL detector.

2.1.1.4 Cylindrical μRWELL studies at TU

Simulation Results

The cylindrical μRWELL simulation study looks at replacing a TPC with a series of cylindrical μRWELL detectors operating in μTPC mode. Additionally, a cylindrical μRWELL could also be used in addition to a TPC to provide a fast tracking element. There were several key goals identified for this funding cycle:

1. Build a prototype μRWELL μTPC to make test measurements which would feed into our μRWELL μTPC simulation, such as the number and resolution of dE/dX measurements based on the angle the track enters the detector and spacial resolutions in the longitudinal and transverse directions.
2. Compare the cylindrical μRWELL performance to that of a TPC.
3. Once the detector is fully simulated this and the forward MPGD simulation work being done by FIT can be integrated into one cohesive tracking simulation.

2.1.1.5 Cylindrical μRWELL studies at UVa

For this cycle, we planned to:

1. **Characterisation of small planar μRWELL prototype:** Study the time and the gain performances and investigate the gain non uniformity observed in previous measurements. We also planned to study the performance of the prototype in high particle flux environment using our X-ray setup.
2. **Build a μRWELL-μTPC prototype:** Assemble a second μRWELL prototype with large drift volume (21 mm instead of 3 mm) and with a built-in field cage for an accurate control of the electric field in the drift region. We will operate the prototype, μRWELL-μTPC in the mini drift mode to explore the single layer tracking capability of this new MPGD technology.
3. **Acquisition of the VMM-SRS electronics:** Complete the procurement the VMM-SRS readout electronics and familiarize ourselves with this new system and its associated DAQ and decoder software. We planned to test the new electronics with the μRWELL as well as with small GEM detectors.

2.1.2 What was achieved?

2.1.2.1 TPC studies at Brookhaven National Lab

As mentioned in the previous progress report, the work at BNL for this reporting cycle was focused on developing the tools required to study aspects of the TPC. Therefore, rather than reporting on a set of performance studies, the following describes several developments and key improvements to our experimental setup.

Cosmic Ray Measurements with TPC Prototype: Although the cosmic ray telescope is a very useful tool to measure reference cosmic tracks for studying the TPC in the lab, it has also become an invaluable instrument for providing extra tracking layers for beam tests conducted at the Fermilab test beam facility. However, each time the telescope is returned to BNL, it must be re-assembled and tested. A single event

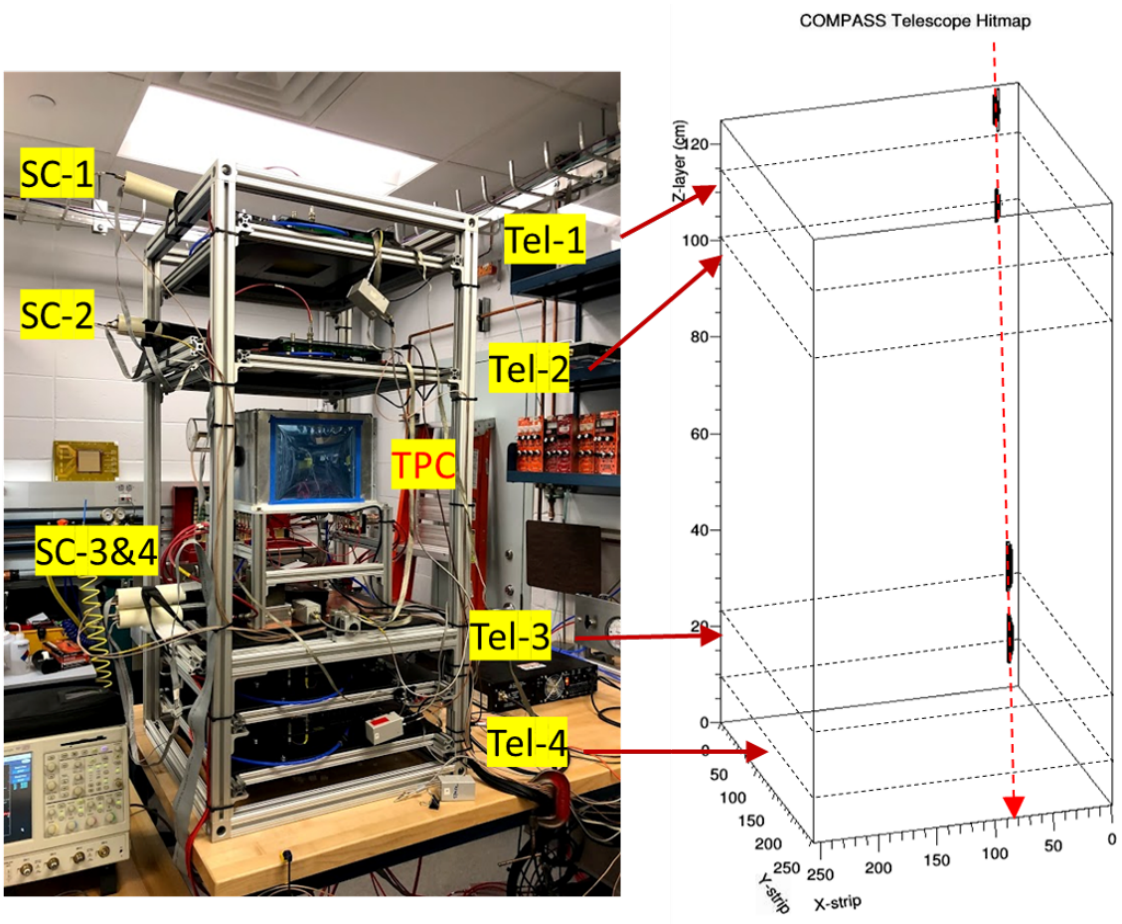

Figure 1: Picture of the "cosmic ray stand" holding the 4 COMPASS based tracking layers. To the right, a single event display shows a charge weighted hitmap for the x,y strips of the COMPASS readout boards in each layer.

display showing a hitmap for the four COMPASS based tracking layers is shown in Fig. 1 after the most recent re-installation several months ago. Particle tracks measured with the telescope provide high resolution reference tracks for studying the response of the TPC to high energy particles measured in the lab. In this case, 16 APV25 cards are read out using the SRS back-plane, for a total of 2048 channels and the usual RCDAQ software is used to record the event files.

There has also been progress on implementing RCDAQ for reading out the SAMPA electronics connected to the prototype TPC. Fig. 2 shows an event display of a cosmic track measured in the 10cm x 10cm x 10cm field cage of the prototype, where scintillation paddles are used to provide the event trigger. In this case, a total of 500 zigzag pads are read out over the full drift time of 12.5 microseconds.

New Zigzag readout PCB for TPC Prototype: In order to proceed with our R&D plans for the TPC prototype, the older zigzag based readout PCB needed to be replaced, primarily for two reasons. The first is the orientation of the pad rows needs to be rotated by 90 degrees so that tracks formed from the laser light setup (described below) are orthogonal to the direction of the pads rows. The alternative would've been to reconfigure the entire apparatus, which is highly prohibitive. The second reason is the zigzag shape for the readout was far from optimized. After spending several years to optimize the geometric parameters that define the zigzag pattern, we have converged on a set we believe should work well for the TPC, so it is natural that the optimized parameter set is employed here as well. It should be noted that the chosen zigzag parameter set is only a best guess since the studies performed so far only employed relatively short

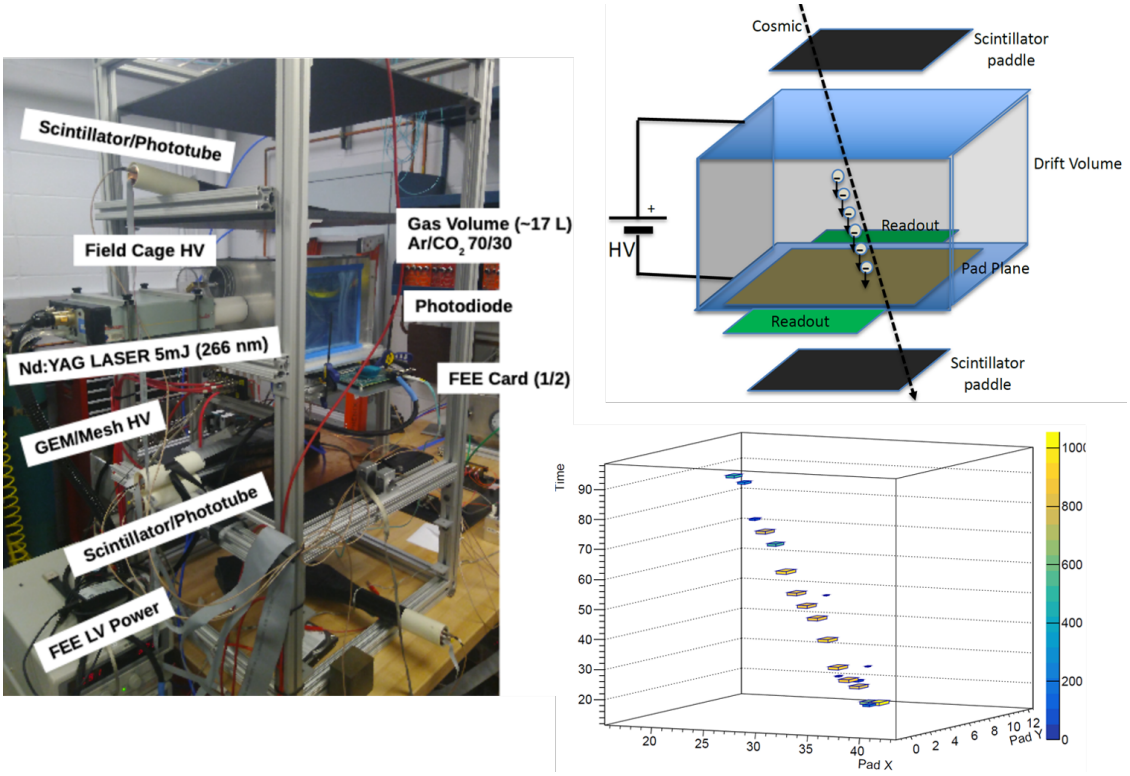

Figure 2: Picture of the same cosmic ray stand in figure 1 (with the COMPASS tracking layers missing), showing the TPC prototype installed in the center as the detector under test. Scintillation paddles are used here to provide the cosmic trigger for collecting charge on the readout plane produced by a high energy particle passing through the field cage. A SAMPA single event display showing the reconstructed position of the ionization charge in the drift volume is shown in the bottom right.

drift distances. In fact, it is a goal of the TPC R&D to determine the most optimal zigzag parameter set for this particular detector configuration.

Some results from the LDRD funded R&D on zigzag shaped readout pads is shown in Fig. 3 and was used to determine the best zigzag pattern to use for the TPC prototype. The data was acquired during a beam test at Fermilab, where a multitude of zigzag patterns were tested with different MPGDs, including a 4-GEM, Micromegas, and μRWELL planar detector. These measurements effectively scan the geometric parameter space of the zigzag and identify an optimal set, which includes the pitch, period, and the degree of interleaving (otherwise referred to as the "stretch" parameter). In addition to achieving the highest position resolution, a major goal of this optimization is to identify zigzag patterns where the response is also uniform across the readout; that is, where there is virtually no differential non-linearity (DNL) present. It must be emphasized that these curves are not in any way intended to be universal, but are specific to the particular detector configurations illustrated in the figure.

The optimal parameter set is generally identified as the set where the pre and post DNL-corrected resolutions are equal, ie where no correction is needed. For the 4-GEM is was found that a pitch of about 2mm, a period equal to 0.5mm, and a stretch equal to 15% would be optimal for the TPC. Interestingly, it was also discovered that larger gaps between adjacent anode pads require larger stretch values for optimal performance. The pitch value was mainly chosen because it is course enough to keep the channel count reasonably low, while maintaining a high resolution, of the order 50 microns (not counting the effects from transverse diffusion). Some of these finding are further articulated in our new paper on zigzag R&D [4], recently submitted for publication in IEEE, TNS.

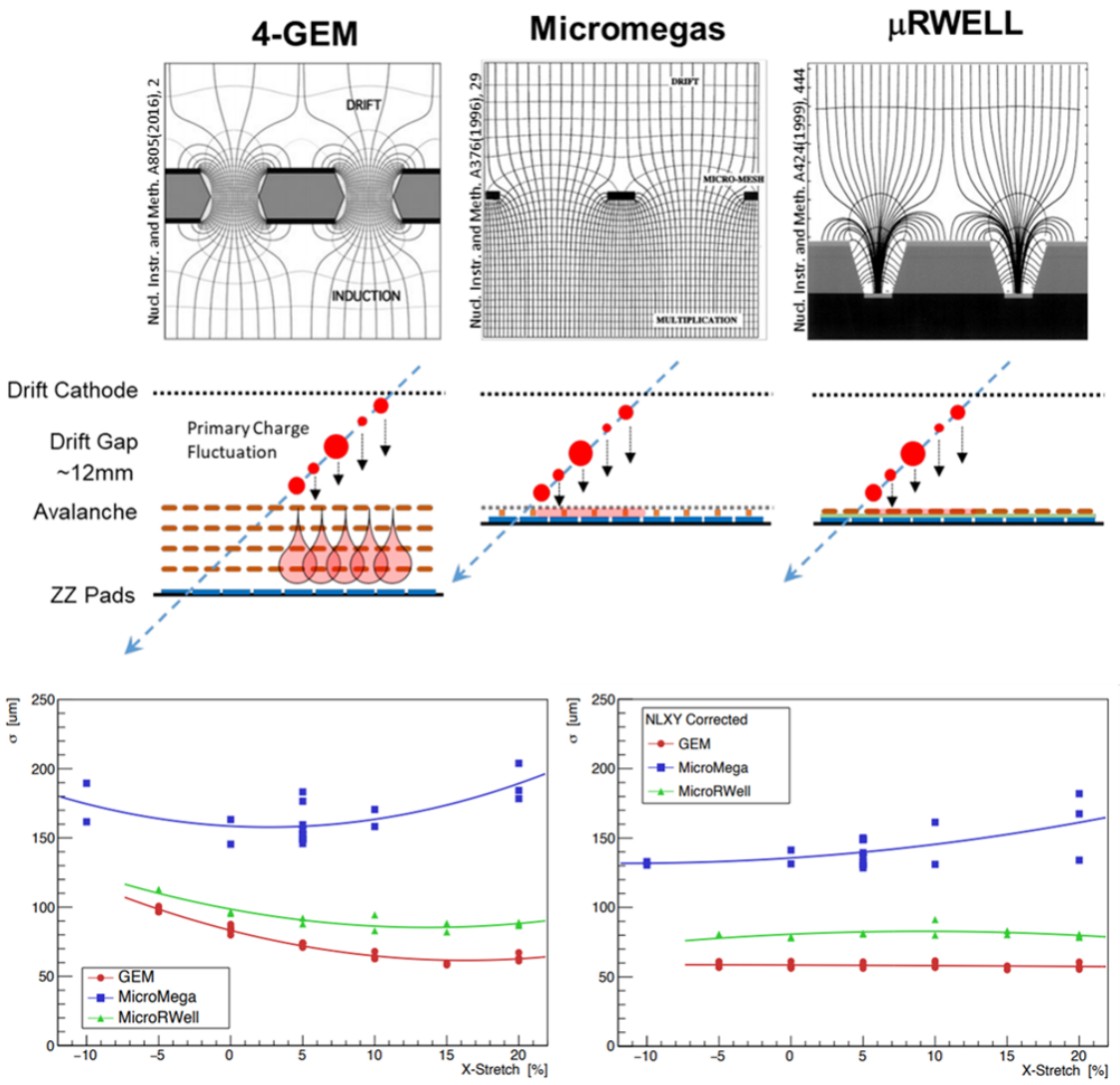

Figure 3: Readout PCB's equipped with zigzag shaped charge collecting anodes were studies with 3 different MPGD avalanche structures, including 4-GEM, Micromegas, and μRWELL. Each detector configuration is illustrated at the top, along with the shape of the respective electric fields. The bottom plots compare the resolution for the three setups as a function of the zigzag stretch parameter. The left plot presents the raw data before a correction for the differential non-linear response of the readout and in the right plot this effect is removed.

A new zigzag PCB has been fully designed and has been submitted to the CERN PCB shop for production. Fig. 4 shows an image of the PCB engineering drawing, including an inset picture of the zigzag pattern employed. For this design, the CERN group is going to use a novel high resolution chemical etching technique in order to generate inter-electrode gaps as small as 2mils (or 50 microns), which should result in a smaller differential non-linearity and higher resolution. The typical industry standard minimum gap width is 3mils (or 75 microns), so there will be some R&D involved with this production, though the CERN group has generated PCBs with such tolerances in the past.

Laser Line Reference Tracks: The standard approach for testing the detector response to lines of ionization generated by high momentum particles is to establish a cosmic trigger using an external detector such as several scintillation paddles. In addition, the means for measuring a reference track entails building

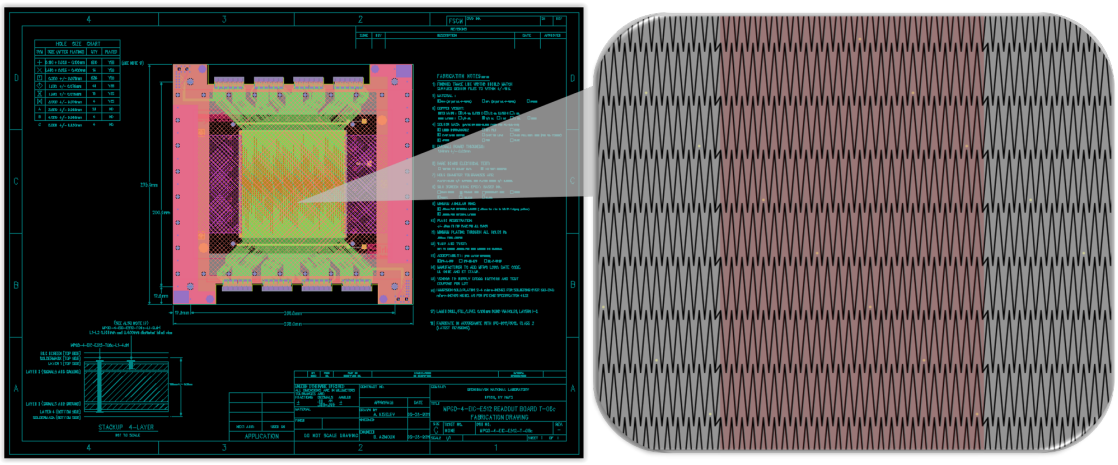

Figure 4: Engineering drawing of zigzag readout PCB for TPC prototype. The zigzag pattern consists of a pitch = 2mm, period = 0.5mm, stretch = 15%, and gap 50 microns. The inset picture of the zigzag pattern highlights a single pad row.

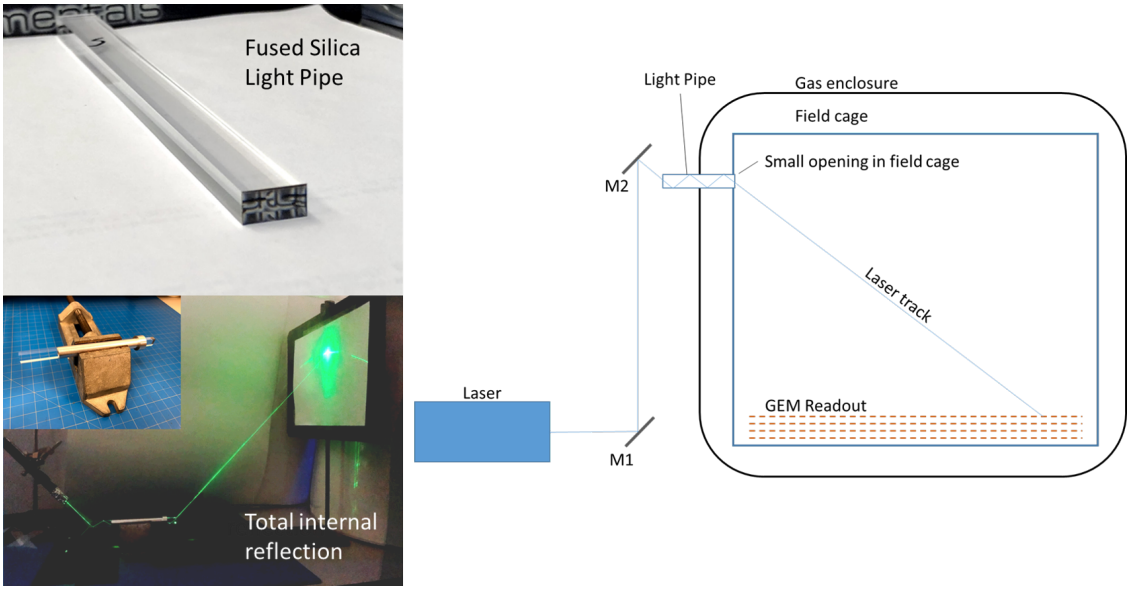

Figure 5: On the left is a picture demonstrating how a laser beam may be redirected using total internal reflection off of the parallel facets of a light pipe. On the right, a sketch of the optical system for the prototype TPC is shown, including the laser, beam steering mirrors, and the light pipe.

a cosmic ray telescope, as was done in our lab. However, this approach has serious drawbacks including the complexities of an additional detector, a limited acceptance, very low data taking rates, and the effect of multiple scattering on track positions and angles. Utilizing laser light to generate lines of ionization within the detector volume has tremendous advantages including, relatively fast data taking rates, a simple trigger (if using a Q-switched laser), no external detectors, fixed and reproducible tracks, and the dE/dx may be tuned by attenuating the light intensity.

As an alternate way of measuring the detector performance, we have developed a novel scheme for delivering laser beams into the TPC volume by exploiting the characteristics of total internal reflection of a light pipe. By controlling the angles at which light is coupled into the light pipe externally, one may steer the angles of the laser beam entering the TPC enclosure (see Fig. 5). This in turn enables the possibility of doing many

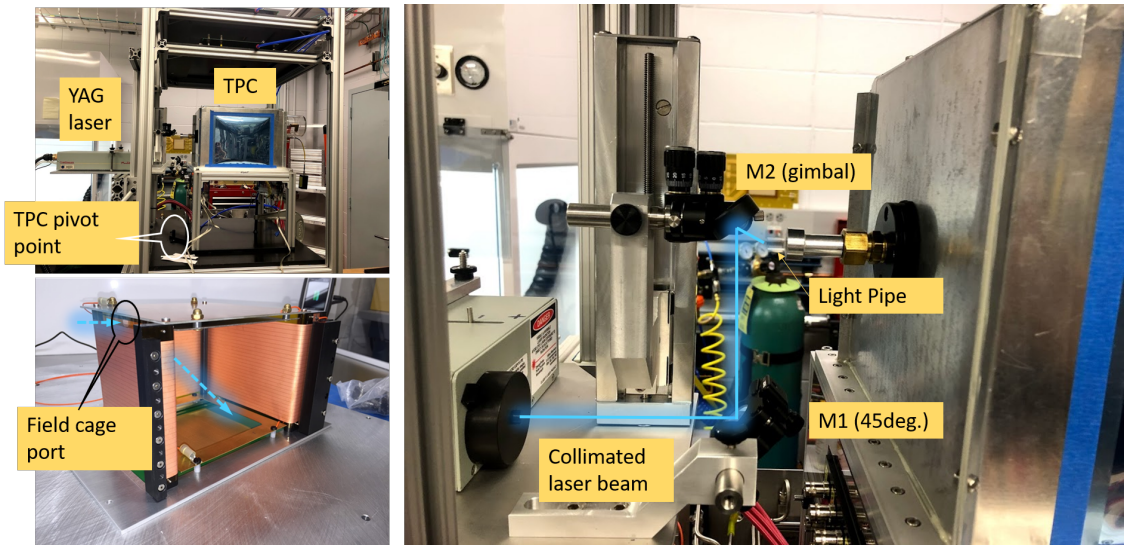

Figure 6: This picture shows the actual components of the optical system for steering the laser beam.

systematic TPC studies using pseudo particle tracks in a convenient way in a lab setting.

By utilizing high energy laser light (such as the 4th harmonic wavelength from a NdYAG Laser, ie 266nm, or 4.7eV photons) a two photon process may ionize trace molecular impurities in the gas, which have ionization potentials in the 9.0 eV range. The gas molecules have ionization potentials of the order of 15eV or more and are not ionized. Typically 20-40μJ/mm$\hat{2}$ is required to have a sufficient probability for the simultaneous absorption of two 4.7 eV photons to initiate ionization. The ionization process is also Poisson, not Landau, so the time profile of the deposited charge looks very different, as seen in the oscilloscope traces in Fig. 8 below. Finally, the rate of ionization goes as the square of the intensity, so the transverse spread of the ionization is significantly smaller than the beam cross section.

Fig. 5 shows a sketch of the optical system used in conjunction with the TPC and Fig. 6 shows a picture of the actual setup. The two polar angles of the laser beam are controlled by a gimbal mounted mirror ("M2") and the pivot angle of the base-plate on which the TPC detector sits.

Fig. 7 shows some ray tracing simulation results to test how well the laser beam can be steered in three dimensional space. In this case, all four facets of the light pipe parallel to the direction of the laser beam are used to bounce the beam in order to provide direction vectors along orthogonal coordinate axes. In this way, the beam may be delivered at virtually all angles making a cone centered on the beam, with a half angle of up to about 85 deg. The light losses on the parallel facets are negligible, however, this depends on the quality and smoothness of the light pipe surface.

Lastly, Fig. 8 shows measurements of the laser tracks using an oscilloscope and the TPC readout electronics. The oscilloscope traces are signals from a preamp + shaper connected to the bottom electrode of the bottom GEM and are useful for conveying the time evolution of the laser signals over the TPC drift time of about 12.5 microseconds. The top trace was recorded using a cosmic trigger and clearly shows clustering in time expected from a Landau process. In contrast, the laser triggered trace on the bottom shows a more continuous deposition of charge over time, which is indicative of Poisson statistics, expected from ionization generated by laser light. The 3D plot on the right depicts a hitmap from laser tracks shooting into the TPC volume. This particular hit map was generated using SRS+APV25 data. Each DAQ frame only spanned a time slice of about 0.6 microseconds, so the full laser track was mapped out by successively increasing the trigger latency.

We have demonstrated that this laser apparatus is viable tool for studying the performance of the TPC using lines of ionization. Due to its convenience and precision, we plan to use it extensively to conduct systematic

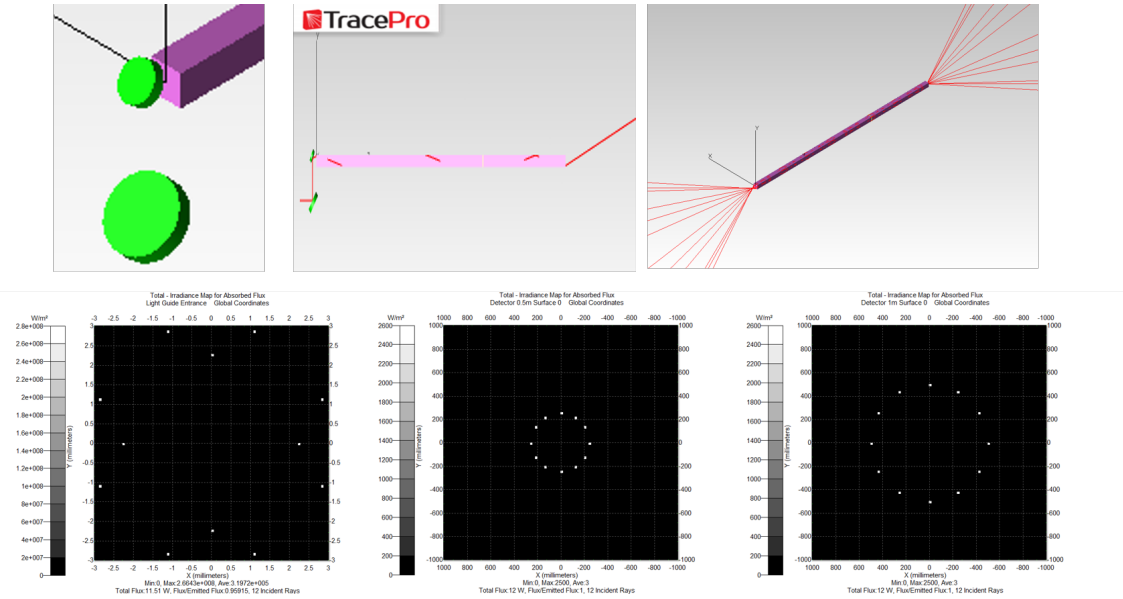

Figure 7: Ray tracing results showing the behavior of the optical system. In this case, the left plot shows the distribution of input points on the entrance facet of the light pipe needed in order to generate a cone of laser beams on a focal plane inside the TCP. The results from two focal planes are shown.

studies of the TPC in the future and we will likely only use the cosmic ray telescope to confirm a small subset of these results with cosmic rays.

High Rate, Narrow Beam X-ray Scanner: We have completed the assembly of our new high intensity, narrow beam x-ray source. After procuring the correct model x-ray tube from the manufacturer, the device was successfully tested on the bench. A full featured control box was then designed and assembled to provide all of the infrastructure services required by the x-ray source, including the power supply, cooling, and the system interlocks. Upon completion, the system was registered and commissioned by the BNL radiological team. The system is now fully operational and we have started to conduct some initial tests with it. The output rate, as measured with the bottom GEM electrode was found to be about 14kHz at 50% power. The size of the beam was not directly measured, but is expected to be about 25 microns x 1mm, based on the size of the slit of the collimator. Unlike our older x-ray source, which outputs a secondary beam from fluorescence from a Mn target, this x-ray source outputs the primary beam from the target anode and has considerably higher intensity due to the fact that it is a 50W tube compared to a 3W tube. The energy spectrum is also highly peaked at the K-alpha energy of the Cu target (8keV), making the output almost monochromatic. Fig. 9 shows some pictures of the overall setup, including the energy spectrum for the primary beam.

Another significant development with this setup is that the DREAM electronics was configured to read out the detector under test. In general, the DREAM electronics provide a high channel count, large dynamic range, and a memory depth of 256 samples, making this FEE system ideal for most applications in the lab (and at a beam test). For this reason, we have made the DREAM electronics portable to be used in multiple detector setups in the lab. The event files are also recorded using RCDAQ, which is a big advantage in terms using a uniform DAQ software for most of our data taking. Fig. 10 shows some initial x-ray scan results from a straight strip PCB. The system is still being configured, so these are only preliminary results. However we expect to have the electronics fully functional very shortly.

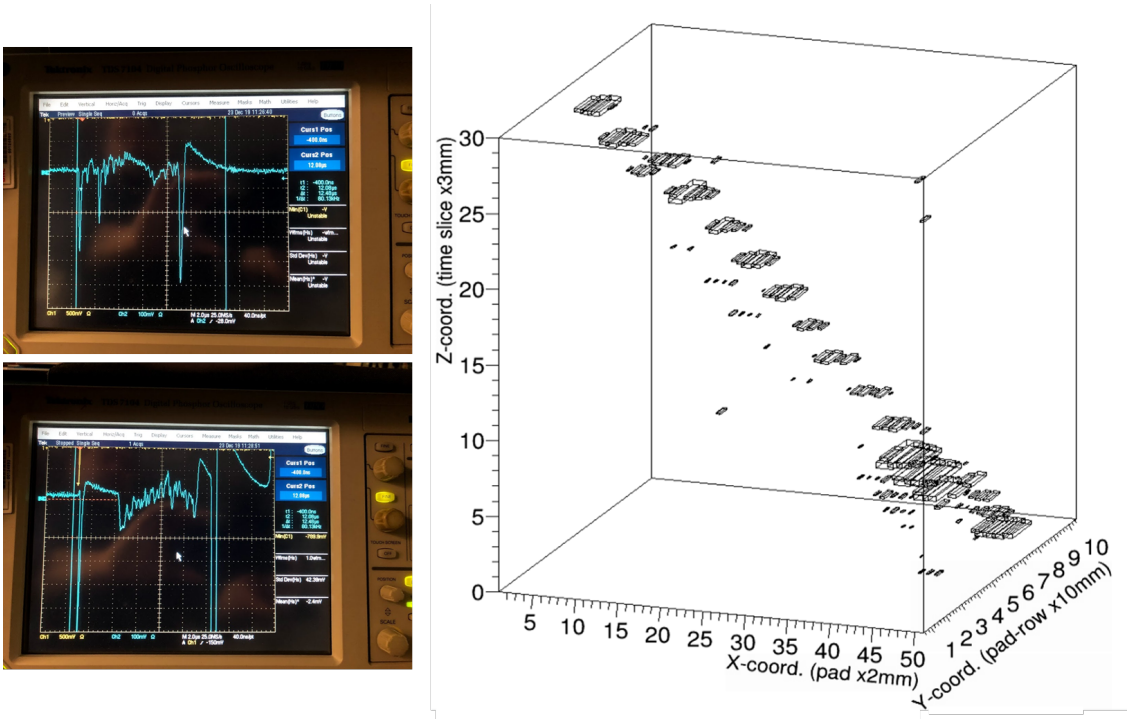

Figure 8: The oscilloscope traces on the left are from signals from the bottom electrode of the bottom GEM foil of the TPC prototype. The top signal was acquired using the cosmic ray trigger and the bottom signal was triggered by the laser. The two signals have very different profiles in time due to dissimilar ionization processes. On the right, a 3D hitmap of a laser track pointed in a fixed direction is shown. Data for each time slice was recorded individually then compiled into a single plot.

2.1.2.2 TPC studies at Stony Brook

In previous TPC applications the problem of charge pile-up due to ion-back-flow (IBF) has been resolved by active gating grids. These grids were actively supplied with a potential over a wire grid that forced ions from the amplification process drifting into the drift volume to be attracted and removed. However, electrons suffer the same fate, hence, this procedure can only be applied at certain periods in time which makes the whole a slow readout device. To overcome this limitation a passive grid design has been investigated.
A setup for a $\sim$30$\times$30 mm^2 opening has been produced (see Fig. 11) for first feasibility studies. The tests are ongoing and we are expecting first results within the next one or two months. We have also designed a wire grid that has a smaller pitch, of $\sim$1 mm, see Fig. 12. This grid will be permanently powered and should provide a way to attract positively charged ions but leaving the path of electrons unaffected when immersed in a magnetic field. Another option is to arrange for a grid of wires separated from each other and apply a constant bias voltage between them (bi-polar grid).
We performed simulations for a variety of configurations in terms of spacing, applied voltages, gas choices, drift-/transfer-voltages. The effect of the passive gating can be seen in Fig. 13 for a specific configuration with T2K (Ar-CF_4-iC_4H_{10} with a ratio of 95-3-2) gas.

2.1.2.3 Cylindrical μRWELL studies at Florida Tech

Conceptual Design Studies for a Full-size Cylindrical μRWELL Tracker: Several design iterations for a cylindrical μRWELL detector were produced using AutoDesk Inventor. The main design principle is still to place all structural support elements at the ends of the cylinders that form the detector segments and at the outside of the detector while the active detection volume is formed only from thin foils to ensure low

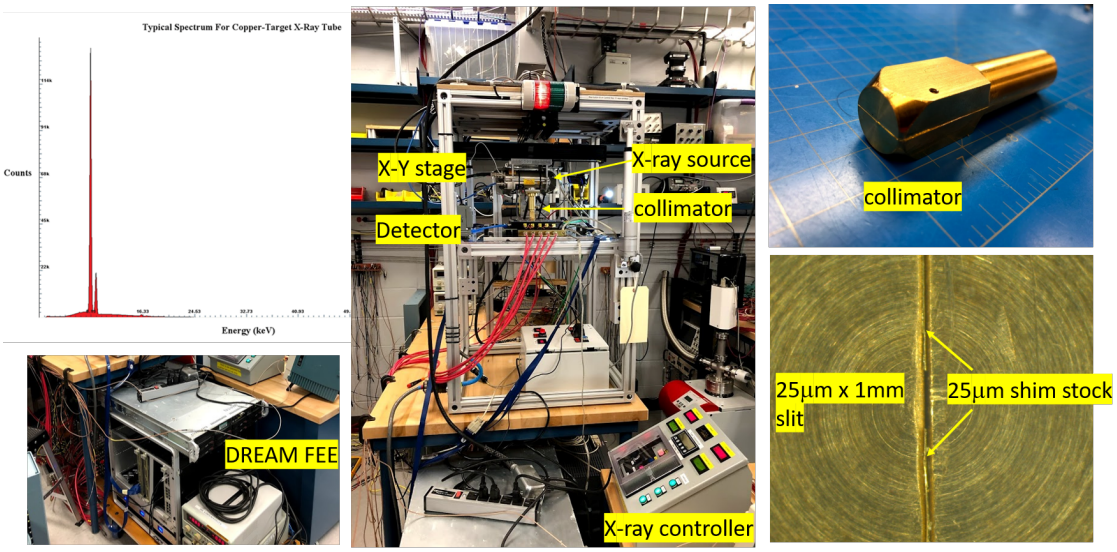

Figure 9: Pictures showing the fully functional x-ray scanner apparatus, including the x-ray spectrum from the x-ray tube, which is equipped with a copper target. Also shown are some details of the construction of the 10cm long solid brass collimator.

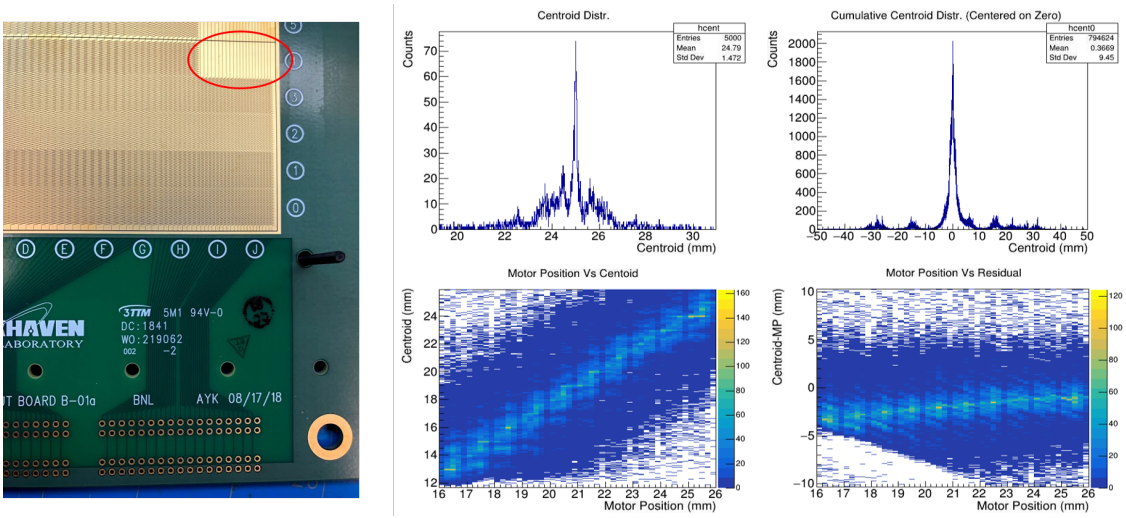

Figure 10: X-ray scan results from straight strip readout pads. The motor position vs centroid plot clearly exhibits a strong correlation, however the resolution plots are not fully valid due to the fact that there are still items that need to be configured with the DREAM system.

multiple scattering in the detector material. A shortcoming of the initial design with three barrel segments were gaps in the acceptance due to non-active regions in the cylinders that are reserved for hosting front-end readout electronics. This is now remedied by radially interleaving adjacent barrel sections so that the active areas in those sections overlap slightly. However, this modification shortens the active detector length in the z-direction too much. Consequently, two more barrel sections are added to the design to ensure full coverage without gaps up to at least $|\eta| \approx 1.0$ and to maintain symmetry about $\eta = 0$ (Fig. 14). In the overlap regions, tracks will encounter more material than in the foil-only regions. The impact of this on multiple scattering and momentum resolution will have to be studied carefully with the simulation being developed by Temple.

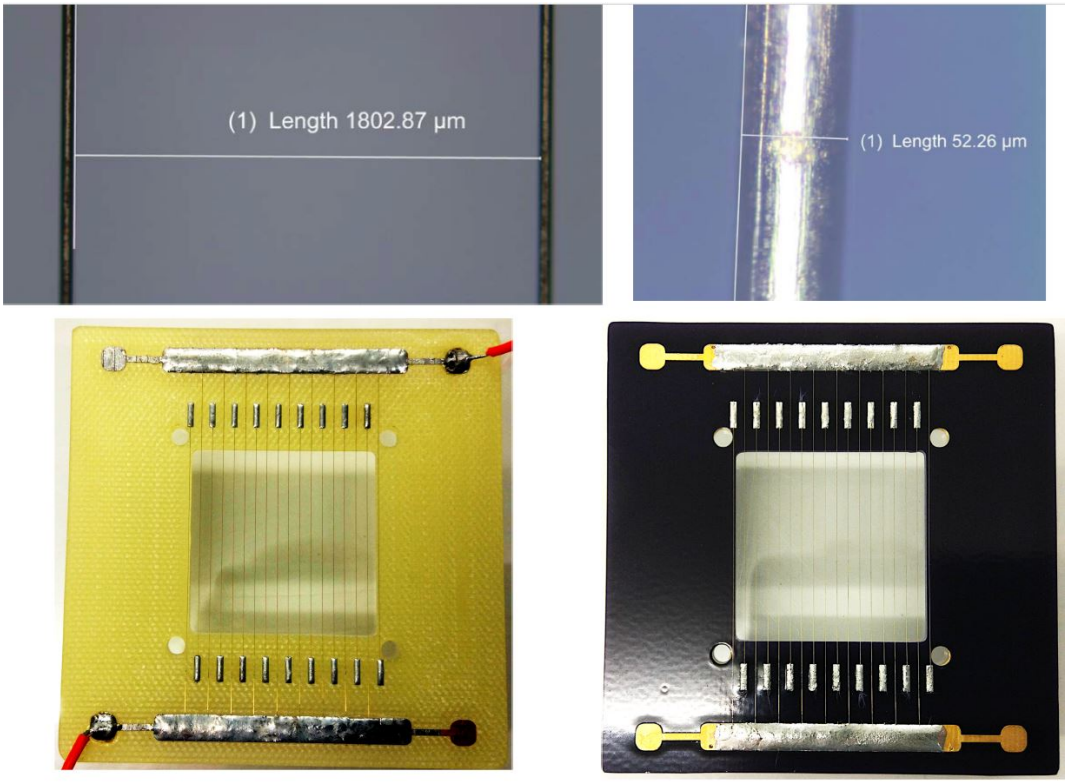

Figure 11: Details of the bi-polar wire grid. Upper row: Left shows the pitch of wires. Right shows the diameter of the wires. Lower row: two masks of different materials with a wire grid at different potentials.

In the previous iteration, the question of how to stretch the central overlapped section of detectors had yet to be answered. We now propose to add long axial stretching rods made from a low-Z material such as nylon that connect the cylinders of the same radius but within different barrel segments to each other and ultimately to the endplates for stretching purposes.

Changes are also made to some size parameters in the most recent design iteration to be more in line with the geometry used in the Temple U. simulations. The design now features μRWELL cylinders with radii of 225.1 mm, 375.1 mm, 475.1 mm, 575.1 mm, 675.1 mm, and 775.1 mm. The drift gaps are changed to 16 mm drift gaps from the 20 mm drift gaps of previous models. The design of the circular carbon fiber frames that allow for simultaneous gripping (on both ends) of the μRWELL foil and the drift foil is updated to include grooves for O-rings to seal the gas volume, as well as slots to place nuts in which to insert and fix the stretching rods, and holes for the clamping screws (Fig. 15).

Mechanical mock-up: We have begun procurement of components for the mechanical mock-up of the smallest detector cylinder. This includes 50 μm kapton foil for the drift foil and 300 μm solid kapton foil to simulate the composite μRWELL/readout foil, 3 mm diameter threaded nylon rods, and adhesive kapton foil for splicing the flat foils into cylinders. The sizes of the frames are adjusted in the design so that we should be able to print them on a 3D printer at the university. We are including gas inlets and outlets in the frames so that we can pressurize the mock-up for leak testing and deformation checks.

2.1.2.4 Cylindrical μRWELL studies at TU

Although we were not able to begin building the μRWELL μTPC due to the delay in processing and receiving our FY20 funding, we were able to continue our simulation studies with the μRWELL cylindrical layers and start to compare its performance to a TPC. These studies are done in EICRoot and have been carried out

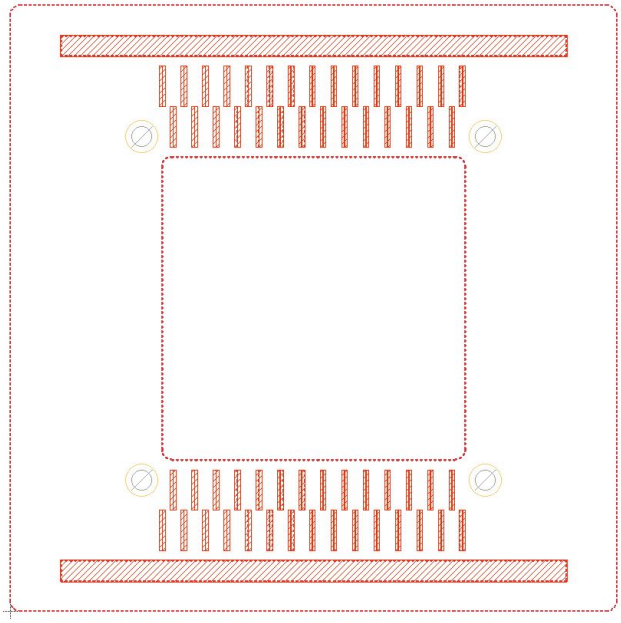

Figure 12: Schematics of a wire grid with alternating voltage between each pair of wires. The soldering pads indicate a positioning aid in form of groves that wires can lay in. The wires are not shown.

predominantly by one of TU's graduate students, Nick Lukow.

Simulation Overview

The μRWELL tracker with 6 equally spaced cylindrical shells is simulated and electrons/pions are simulated passing through the detector at various energies and angles. Each μRWELL layer registers a single hit point, which is then smeared longitudinally and azimuthally. The amount of smearing is varied to simulate μRWELL layers with a variety of single hit point resolutions: 100 $\mu m\times$ 100 μm, 150 $\mu m\times$ 150 μm, and 200 $\mu m\times$ 200 μm. The reconstructed track parameters are extracted from the track at a point just outside the tracker. These extracted parameters are compared to the true Monte Carlo track parameters to find the residuals of the track parameters (polar angle, azimuth angle, and momentum).

Alongside the studies with the μRWELL, a TPC simulation based on the sPHENIX TPC is also performed. The same track parameters are investigated, and the residuals are compared to the μRWELL values. This is done to compare the performance of the μRWELL design to that of a TPC.

Tracking Performance

The momentum resolution for 6 GeV electrons in a 1.5 T field were simulated for both the μRWELL tracker and TPC and are shown in Fig. 16 as a function of the polar angle. The μRWELL performance was studied using three different sets of spacial resolutions. Overall the TPC displays the better momentum resolution, but is very comparable to the μRWELL with spacial resolution of $100\mu m\times$ $100\mu m$. In particular the TPC performs better than the μRWELL at smaller polar angles, around 45^o, and is slightly out performed by the μRWELL at larger angle (65^o).

Figure 17 studies the corresponding polar angle resolution of the two detectors. From this study we see that the μRWELL provides better angular resolution compared to the TPC. The angular resolution of the TPC is seen to have some angular dependence, with the resolution improving as the polar angle increases. Where as the resolution measured by the μRWELL appears relatively constant over a wide angular range.

Material Budget

The material budget related to the TPC (left panel) and the 6 layers of the μRWELL tracker (right) has also

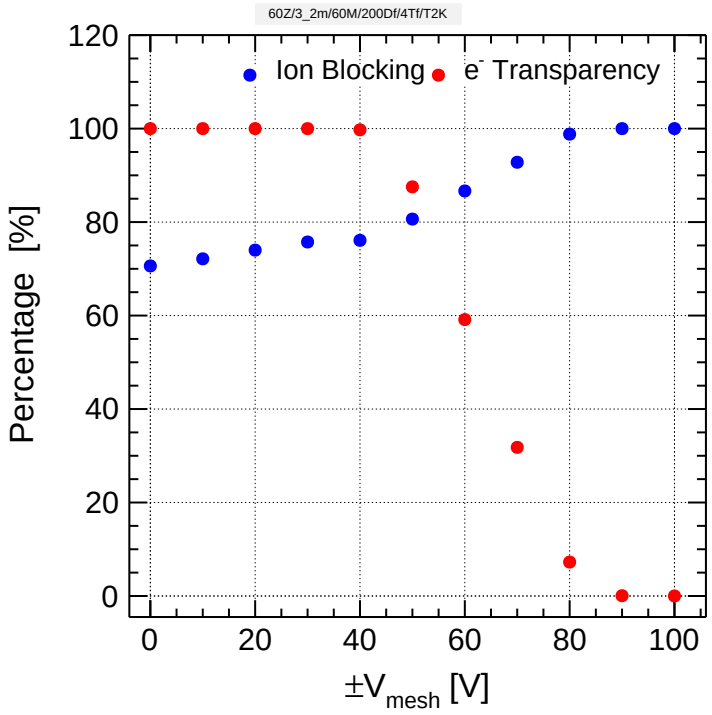

Figure 13: Effect of a bi-polar wire grid for a specific configuration in T2K gas. The IBF blocking effect is very promising at an applied voltage of ±50 V across a pair of wires.

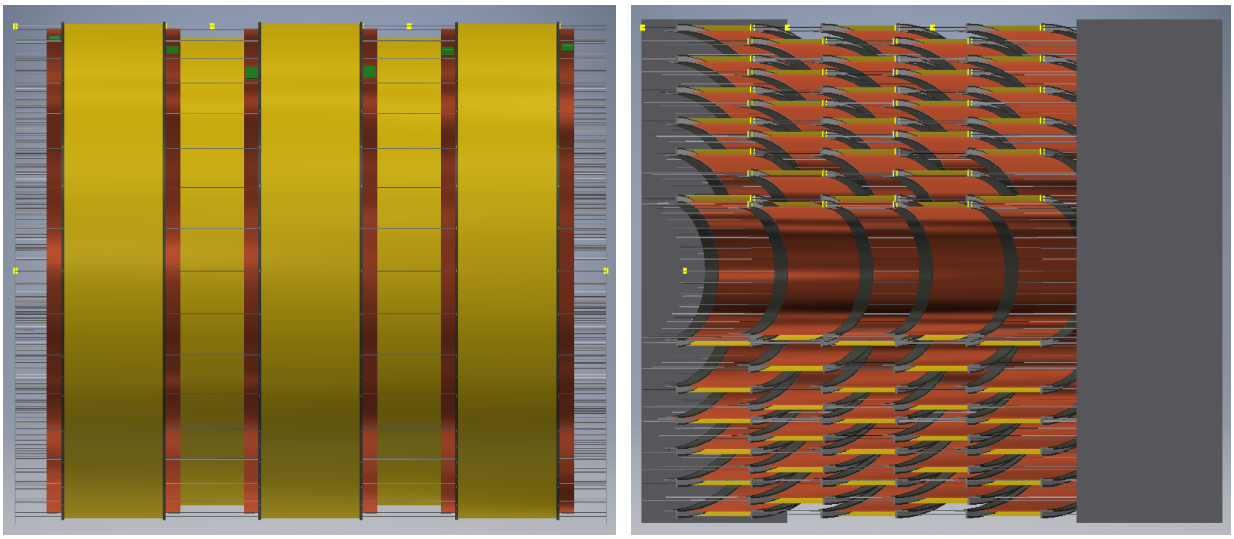

Figure 14: Left: Updated conceptual design of central μRWELL detector with five barrel segments. Right: Longitudinal cross-section view of this multi-segment configuration showing the staggered arrangement of radial detector layers to achieve full geometric acceptance. Endplates shown in gray provide the mechanical support.

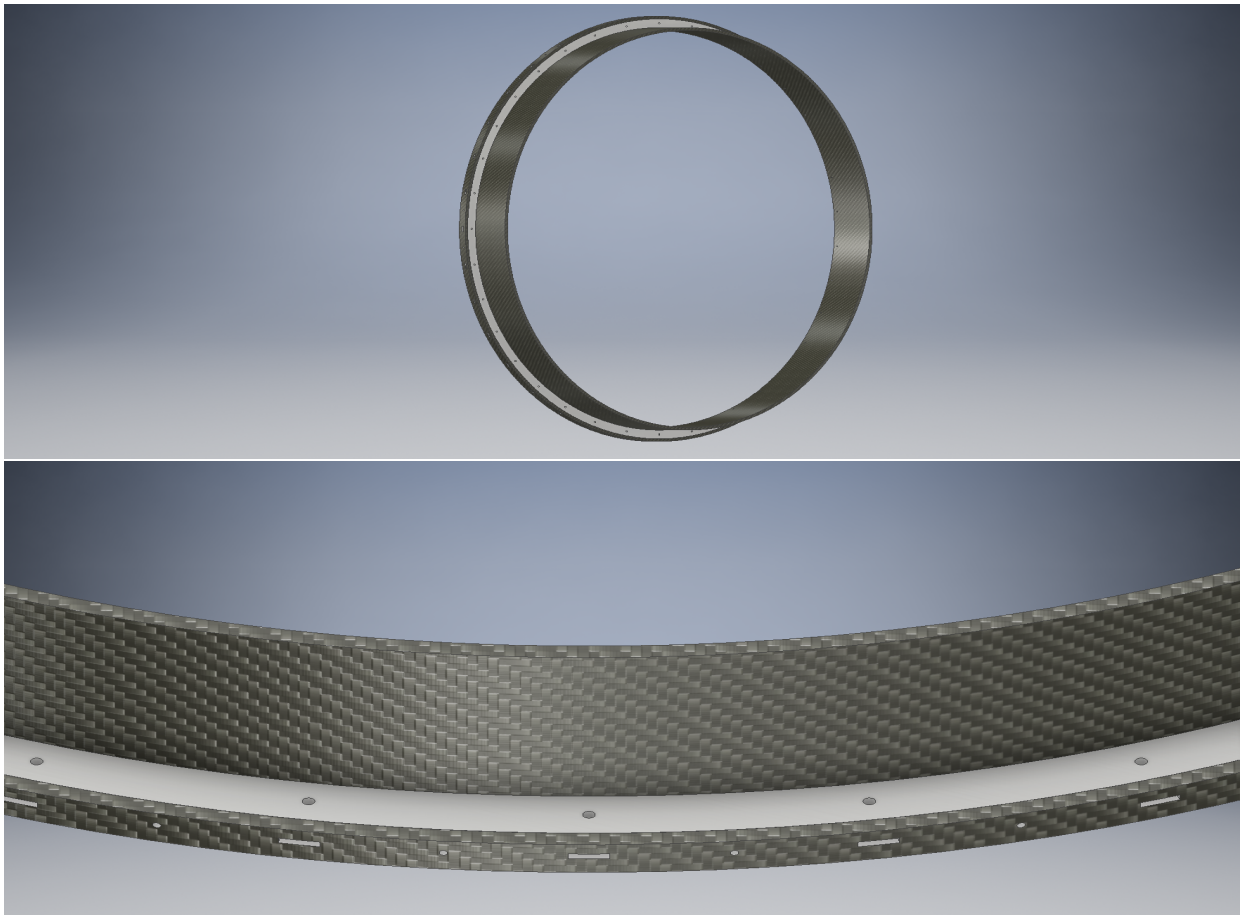

Figure 15: Top: Full view of carbon fiber frames for clamping μRWELL and drift foils and supporting front-end electronics in the cylindrical μRWELL design. Bottom: Zoomed view of frames with details of holes for stretching rods, slots for inserting embedded nuts, and holes for clamping screws.

been studied and is presented in Fig. 18. From this study we see that the 6 layer μRWELL tracker has a larger material budget than the TPC. The dominant material in the μRWELL tracker material budget is from the PCB board that the μRWELL foil and readout are mounted to. This can be seen in the cartoon shown in Fig. 19. We are currently pursuing studies on how to reduce this PCB material and also investigating the impact of the material on the tracking performance.

PID Input

To help guide some of our studies we have begun discussions with the PID consortium to better understand the tracking requirements they need for particle identification, in particular with the DIRC. Through these initial discussions we have learned that for particle ID with the DIRC, which will be located outside the central tracker, the most important tracking requirement is to have excellent polar angle resolution ($\sim$1-0.5 mrad). We do intend to meet again with DIRC representatives once we have completed tracking studies performed at the DIRC location to discuss our findings.

2.1.2.5 Cylindrical μRWELL studies at UVa

1. **Characterisation of small planar μRWELL prototype:** We had the opportunity to install the μRWELL prototype in test beam in Hall D at JLab this Fall 2019 behind Hall D spectrometer. The test beam is originally aimed at the commission of a DIRC detector for Hall D detector upgrade. The μRWELL

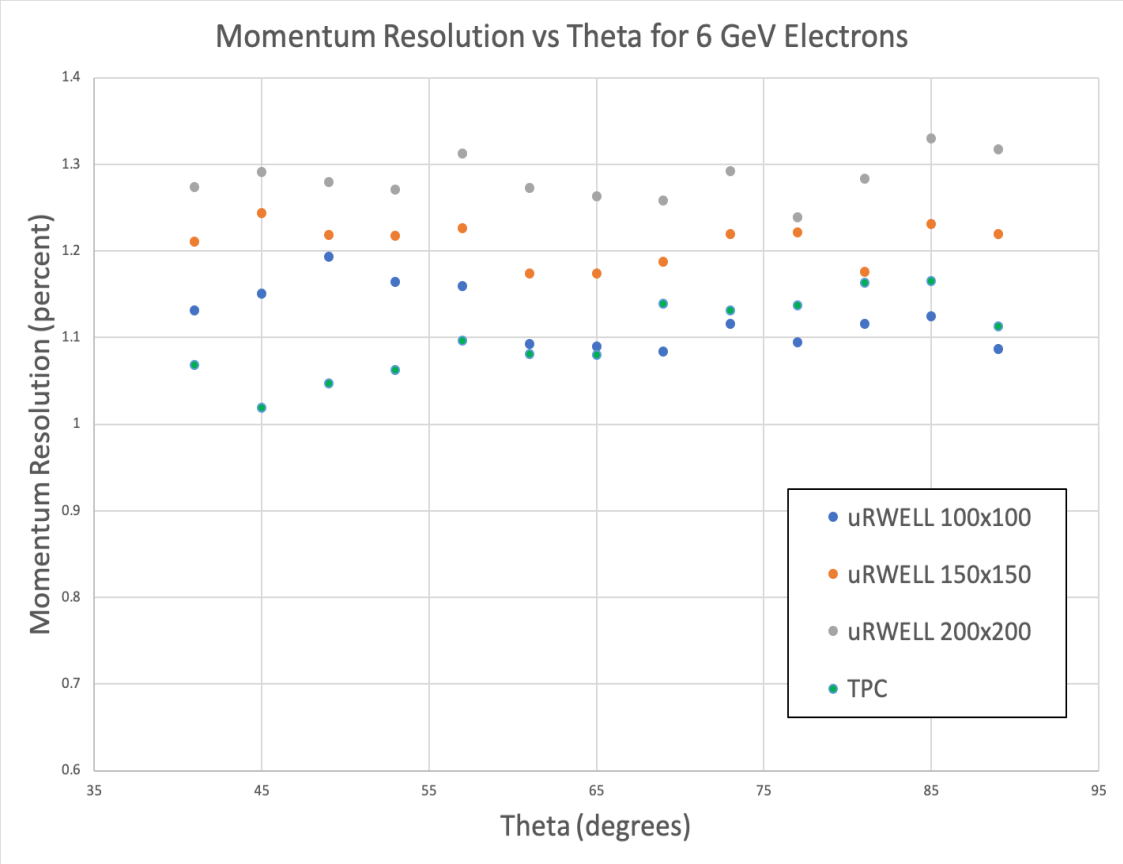

Figure 16: Comparison of the momentum resolution obtained from μRWELL and TPC simulations vs. polar angle. The μRWELL performance was evaluated using several spacial resolution values.

prototype, together with two other standard small triple-GEM detectors and the GEM-TRD prototype developed for the eRD22 R&D effort were added to provide accurate tracking and PID information for the analysis of the DIRC data. Fig. 20 shows the Hall D test beam setup. We will use the test beam opportunity to study the performances of the μRWELL prototype such as the efficiency and gain uniformity with electrons and charged pions as a function of the applied HV. The test beam is currently ongoing and we expect to start looking at the first data for analysis in January 2020.

2. **Build a μRWELL-μTPC prototype:** We have completed the design of the μRWELL-μTPC prototype with the technical support of the MPGD experts from the CERN PCB workshop. This second μRWELL prototype will be built with a long drift gap of 20 mm instead of the 3 mm typically used for a standard tracker, to allow the detector to operate in a mini drift or micro TPC mode where a single detector layer provides enough space points information to reconstruct the track of a charged particle. A preliminary sketch of the cross section of the μRWELL-μTPC prototype design is shown on Fig. 21. The production of the parts at CERN is expected to start early next year soon after the paperwork for the FY20 funding is completed and the assembly and preliminary tests at UVa in the first half of 2020.

3. **Acquisition of the VMM-SRS electronics:** We have received most of the components of the VMM-SRS readout electronics purchased from the SRS-Technology company and and the CERN store. The small system of 512 electronic channels is composed of 4 SRS-VMM hybrids front end cards (VMM-SRS FE cards), the digital card (SRS-DVM board), the data concentrator board (FECv6-SRS board) an upgraded version of the ATX power supply crate. Fig. 22 shows some pictures of the different elements of the system. The picture on the top right of Fig. 22 shows the Hirose-To-Panasonic adapter board required to interface the VMM-SRS FE cards with the new 130-Pins Hirose connectors to existing MPGD detectors

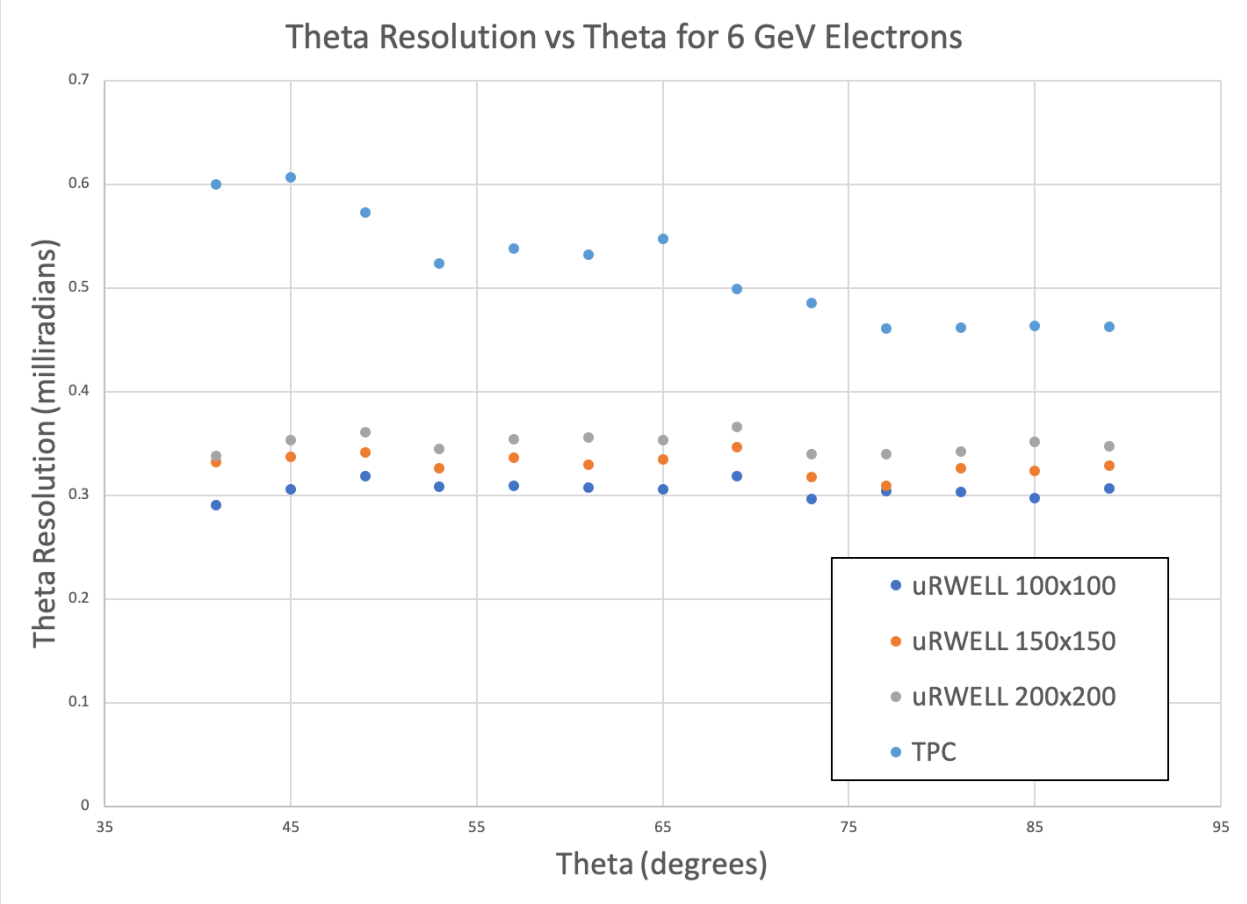

Figure 17: Comparison of the polar angle resolution obtained from μRWELL and TPC simulations vs. polar angle. The μRWELL performance was evaluated using several spacial resolution values.

with the standard 128-pins Panasonic connectors. We are waiting for the delivery of the ATX SRS power supply crate to start testing the new electronics. The procurement of this components has been delayed due to some production issues from the CERN store.

2.1.2.6 GEM CCD Scanner at TU

GEM CCD Scanner

The large area GEM CCD scanner at Temple University continues to serve the MPGD community. We recently completed scans of a μRWELL foil and are in preparations to scan a Low Temperature Co-fired Ceramic (LTCC) GEM.

μRWELL Foil

At the end of last summer we had received a μRWELL foil, which had not been mounted to a PCB/readout board, from FIT to scan with our GEM CCD scanner. This foil was identified by CERN as having known production issues associated with it. Because the 'holes' of a μRWELL foil are actually wells, which are not completely etched through the foil, we are not able to measure the inner diameter of the well. To measure inner diameters we rely on the light from our back light to travel through the 'holes' and reach our camera.

However, we were able to scan the outer hole diameters and their pitch. The left most panel in Fig. 23 shows the μRWELL foil on the GEM CCD scanner. The pitch (middle top panel), hole diameter (middle

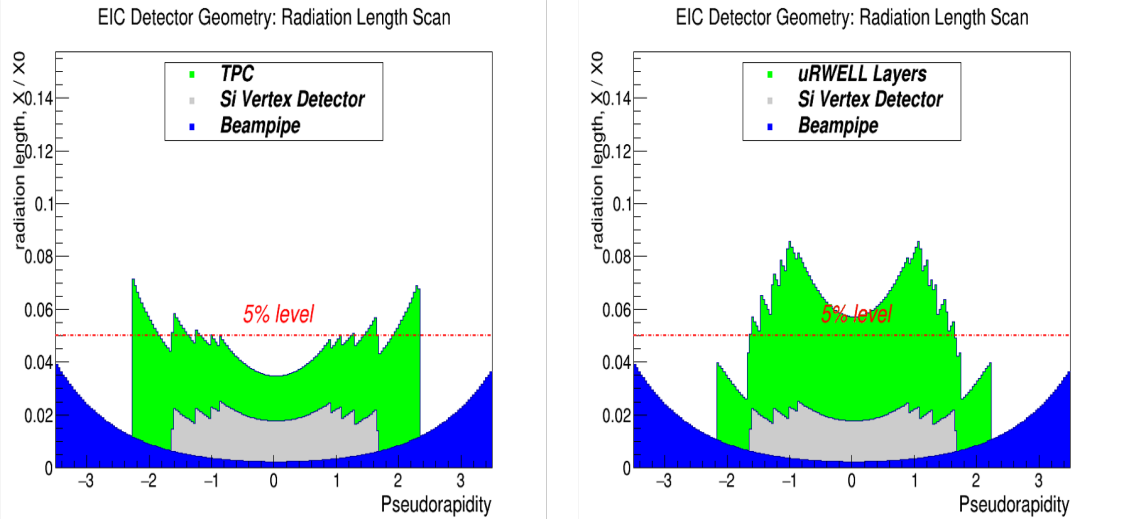

Figure 18: Comparison of the material budget for the TPC (left) and 6 μRWELL layers (right) which are used in our current simulation.

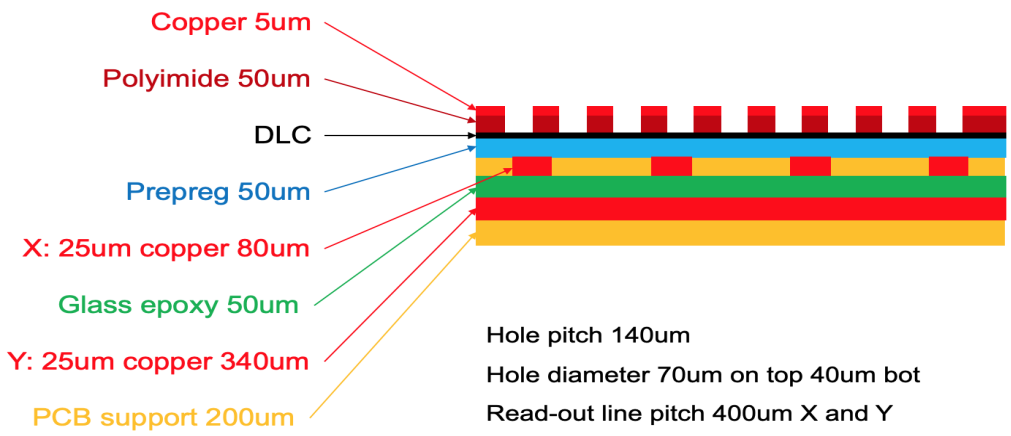

Figure 19: Cartoon of the material making up a μRWELL layer.

bottom panel), deviation of the hole diameter from the mean value over the area of the foil (top right panel), and the hole diameter deviation from the mean (bottom right panel) of the outer diameter scan results are also shown in Fig. 23. Overall, the foil showed mean pitch ($\sim$140 μm) and outer diameter ($\sim$60 μm) values typical of standard GEMs, and were uniform across the entire foil.

LTCC GEM

TU has recently been contacted by some BNL colleagues inquiring if our GEM CCD scanner would be able to perform an optical analysis of a LTCC GEM as a means to investigate gain uniformity. These GEMs are 100 μm ceramic sheets plated by gold on both sides, containing 100 μm diameter cylindrical holes with a pitch of 200 μm. Figure 24 shows an image of the LTCC-GEM. With the GEMs reflective gold coating, we should be able to image the GEM's hole diameter and study its variation across the area of the GEM. We are currently waiting on BNL to complete gain measurements of the LTCC-GEM, then they will ship us the framed GEM, where we will scan it with our CCD scanner and study the hole uniformity of the GEM.

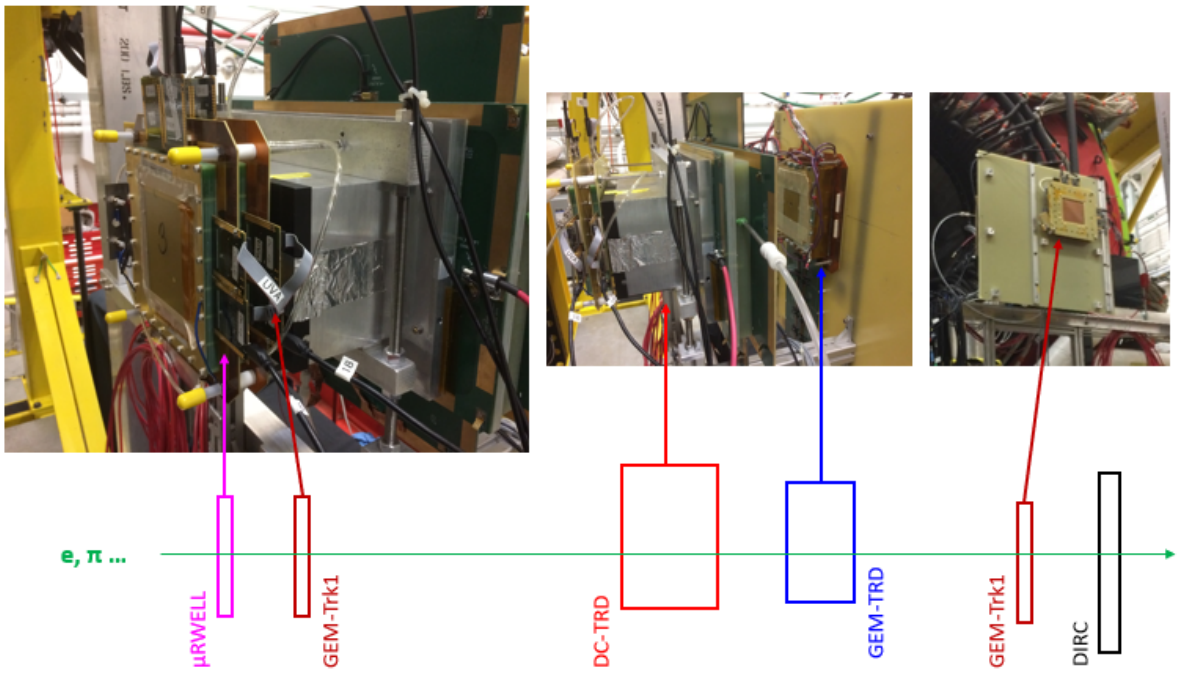

Figure 20: The μRWELL prototype in the Hall D test beam setup at JLab in Fall 2019.

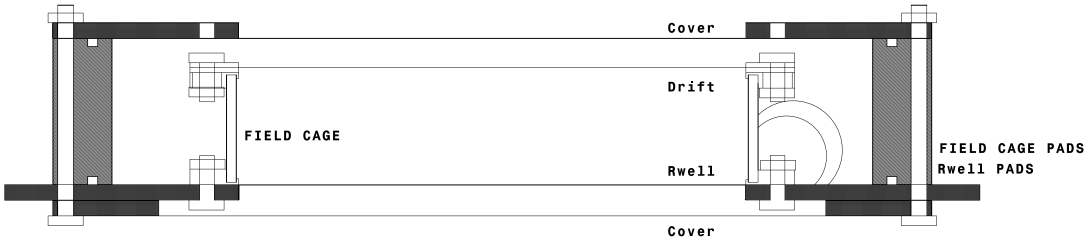

Figure 21: Sketch of μRWELL-μTPC prototype with a 20 mm drift region and built-in field cage.

2.1.3 What was not achieved, why not and what will be done to correct?

2.1.3.1 TPC studies at Brookhaven National Lab

Although we had originally planned to take more data with the 4-layer cosmic ray telescope to study the TPC, we have become less focused on using this instrument since the laser system described above provides significant advantages over reconstructing cosmic tracks. As a result, we have redirected our efforts to developing the laser system, which we believe will ultimately provide most of the data for the TPC R&D. However, it must be noted that we do still plan on using the cosmic ray telescope to validate the response of the TPC to high energy particles in the lab. For this reason, we plan to continue improving and tuning the tracking capabilities of the telescope. In addition, the cosmic ray telescope layers make excellent tracking layers for a beam test.

2.1.3.2 TPC studies at Stony Brook

The technical implementation of a passive gating grid has yet to be performed. The work on this project is ongoing.

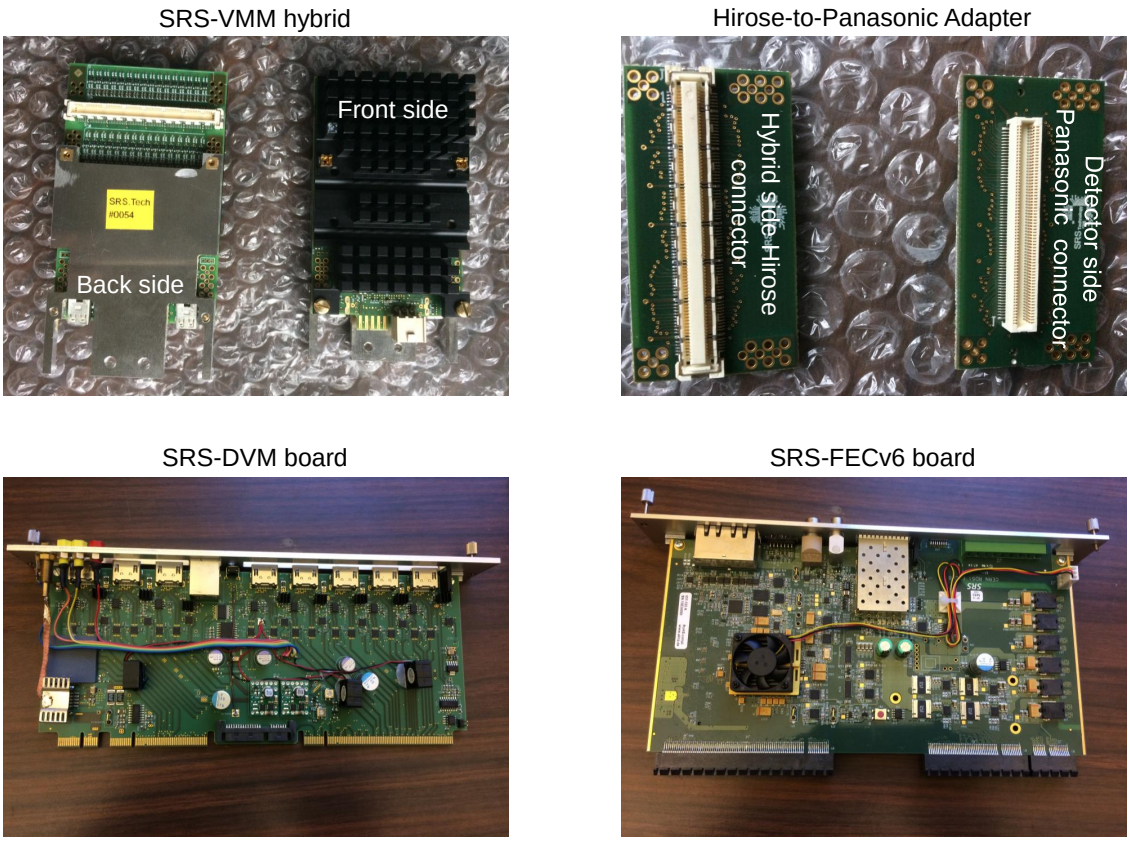

Figure 22: Main components of the UVa small scale SRS-VMM readout electronics system. *top left:* The SRS-VMM hybrid with its cooling structure on both front and back side; *top right:* Hirose-To-Panasonic adapter cards for MPGDs with Panasonic connectors; *bottom left:* SRS-DVM card and *bottom right:* SRS-FEC card.

2.1.3.3 Cylindrical μRWELL studies at Florida Tech

Due to a change in students working on the 10 cm $\times$ 10 cm μRWELL prototype, we have not yet been able to establish signal in this detector and to commission it.

2.1.3.4 Cylindrical μRWELL studies at TU

We have not yet procured the materials to build our μRWELL μTPC due to delays in having the awarded FY2020 money available.

Once the awarded money is available we will place our μRWELL μTPC order with CERN.

2.1.3.5 Cylindrical μRWELL studies at UVa

1. **Characterisation of small planar μRWELL prototype:** The characterisation of the μRWELL prototype is still ongoing. The prototype has been installed in test beam in Hall D at JLab for efficiency study as well as the detector timing and gain uniformity response. Analysis of the test beam data is expected to take place in the first half of the cycle.

2. **Acquisition of μRWELL-μTPC prototype:** The basic design of a second μRWELL prototype is

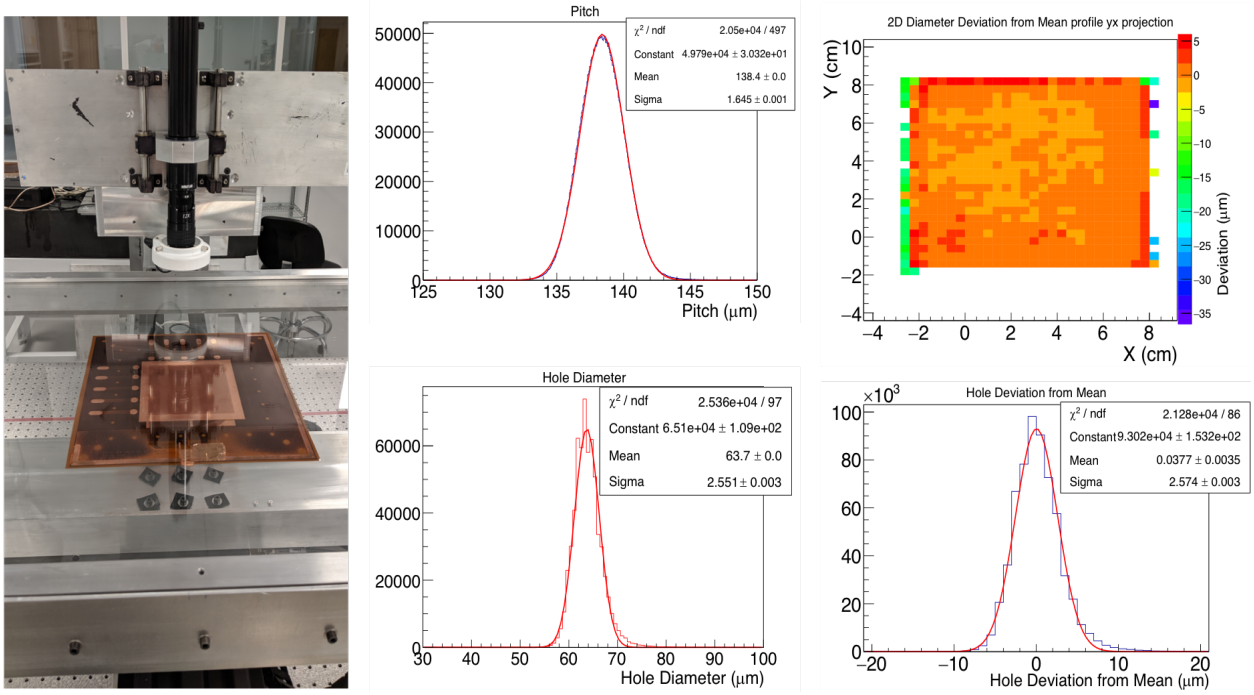

Figure 23: Results of μRWELL foil CCD scan.

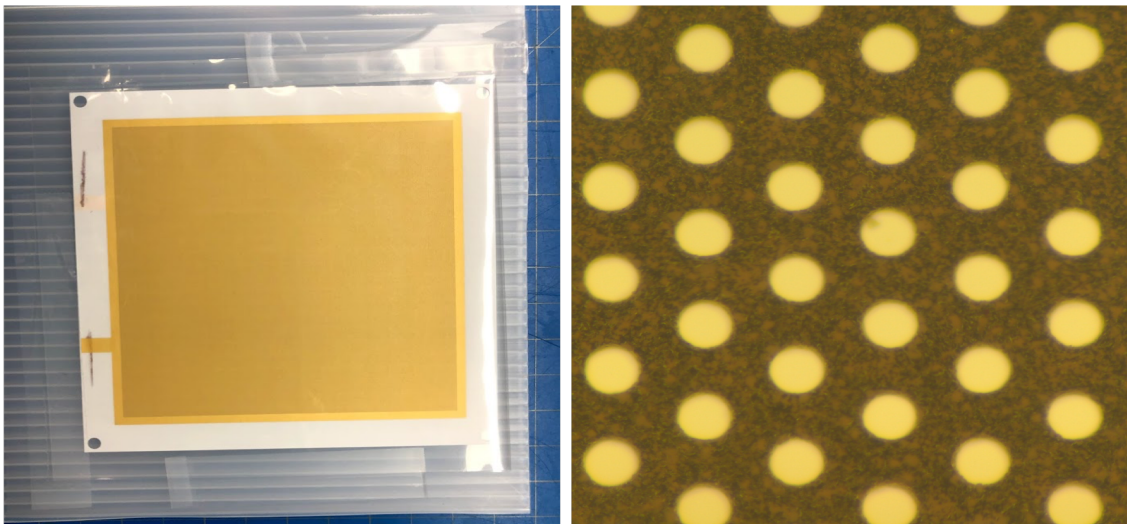

Figure 24: LTCC-GEM (left) and close up of it's hole pattern (right).

completed and we are waiting for the awarded funding for FY2020 to start the procurement from CERN of the parts and to assemble the prototype.

3. **Acquisition of VMM-SRS electronics:** Some parts of the VMM-SRS readout electronics such as the ATX power supply crate have still not been delivered to us. The delay is due to production issues at CERN. We are waiting for the shipment of these critical items to start the assembly of the system and the training to familiarize with the new readout electronics

2.1.4 What is planned for the next funding cycle and beyond?

2.1.4.1 TPC studies at Brookhaven National Lab

Our proposed R&D activity for the next funding cycle is as follows:

- Procure new TPC zigzag PCB and start studying the detector response using the new laser system. If time permits, we also plan to outfit the new PCB design with Micromegas and μRWELL MPGDs. Finally, we plan on reading out the prototype with both SAMPA and DREAM FEE.
- Start using the new high intensity, narrow beam x-ray source to measure the response of new zigzag patterns for potential use in the TPC. Time permitting, the new TPC readout boards equipped with a 4-GEM, Micromegas and μRWELL will all initially be scanned with the x-ray scanner prior to being installed in the TPC prototype. We plan to use the DREAM and possibly SAMPA FEE to read out the detectors.

Long-term goals:

- Continue to optimize and tune the cosmic ray telescope system and the associated software.
- Further tests with the TPC prototype will include testing zigzag readout patterns optimized for a TPC; testing different avalanche schemes in the TPC (eg. Micromegas, and μRWELL); testing promising gas mixtures; and measuring the charge spread, attachment, and IBF.
- Simulation studies of the response of various zigzag readout patterns in combination with different detector gases and avalanche technologies for a TPC.

2.1.4.2 TPC studies at Stony Brook

The implementation of a passive gating grid and its investigation is highest priority for the study of TPC optimization at SBU.
We are working on the design of a wire grid that will be placed upstream of a readout structure and can be placed in a TPC prototype. Subsequently, we are planning to move this setup to the high magnet setup at Argonne National Lab in order to test the ion-blocking feature in a B = 1.4 T environment. This test would serve as a real test under conditions, for instance, as foreseen with an implementation in an EIC detector based on sPHENIX.

2.1.4.3 Cylindrical μRWELL studies at Florida Tech

We plan to start the construction of the mechanical mock-up of the smallest cylinder in the tracker barrel. The main motivation is to check if foils can be properly stretched according to our design to produce a stable and uniform cylindrical structure from foils. One concern is that two ends of a commercial foil coming off a roll must be spliced together to form a cylinder. We will investigate how best to implement this splicing to get uniform foil cylinders. If we can successfully build one such cylindrical segment, we will add two more segments in the same way to create a mock-up of one full cylinder of the three-segment structure envisioned in our design. The purpose is to study if the foil stretching still works if three segments are connected together and stretched only from the ends.

2.1.4.4 Cylindrical μRWELL studies at TU

For the remainder of this funding cycle we plan to

1. Build and measure performance of μRWELL μTPC to feed into our simulation. This will allow us to make measurements of the number of dE/dX points, their resolutions, spatial and timing resolutions, and how they depend on the angle the track enters the detector. This prototype detector will be a planar 10 cm x 10 cm μRWELL detector with a 15 mm drift gap that we will operate in a μTPC mode. We will use CERN's μRWELL kit, where they will modify the frames so that the drift gap is 15 mm. The detector will be readout making use of the APV based SRS system.

2. Continue our μRWELL tracker simulation by completing the following studies

   - Investigate the effectiveness of extra tracking layers behind the DIRC.
   - Optimize the number of layers in our μRWELL tracker and their spacing.
   - Currently our simulation uses one large cylindrical μRWELL foil per layer, though in reality this will be segmented. This segmentation will also need to be implemented in the simulation.
   - The simulation also currently only registers a single hit point per μRWELL layer, whereas in reality, the μRWELL layers will be able to operate in a μTPC mode which will give track segments at each layer which will be used to reconstruct the full track. This has yet to be implemented in the simulation.
   - Implement the μRWELL support structure that FIT is designing.

2.1.4.5 Cylindrical μRWELL studies at UVa

For the coming cycle of FY20 and beyond, we plan to:

1. **Characterisation of μRWELL prototype:** Continue the characterisation of the prototype, and more specifically investigate further the time properties and the non uniformity pattern observed with this detector. We will analyse the JLab Hall D test beam data to extract the efficiency performances of the prototype. We also plan to study spatial resolution and timing characteristics of the prototype in the cosmic stand with small GEM trackers setup that we are assembling at UVa. Moreover, we will take advantage of the upcoming FNAL test beam test opportunity in March 2020 by our BNL colleagues (B. Azmoun and A. Kiselev) to commission the prototype even further in hadron beam environment.

2. **Assembly and preliminary tests of the μRWELL-μTPC prototype:** Complete the procurement of the parts for the μRWELL-μTPC prototype from CERN and assemble the detector. We will then perform preliminary tests the prototype. Finally, we plan to instrument the prototype with the new VMM-SRS electronics to study its performances in the mini drift operating mode and perform comparative study with the TU μRWELL-μTPC prototype constructed without field cage. This study will inform us on the necessity to instrument a μRWELL-μTPC with a field cage to improve single layer tracking ability of such detector.

3. **Assembly and preliminary tests of the VMM-SRS readout electronics:** Complete the procurement the minimal VMM-SRS readout electronics and familiarize ourselves with this new system and its associated DAQ and decoder software. We plan to test the electronic with the μRWELL prototypes and specially testing performances of the system when operating the μRWELL-μTPC prototype in mini drift mode. Finally. we plan work together with BNL colleagues (M. Purshke) to integrate the new readout system into the RCDAQ data acquisition framework use by the larger EIC tracking detector R&D community.

2.2 Forward Tracker

Here, we present a brief introduction of the R&D effort conducted by three institutes, Florida Tech (FIT), University of Virginia (UVa) and Temple University (TU) to design, prototype and characterize GEMs for the forward tracking system of an EIC detector. The primary focus of the R&D program is on the

	Status of the prototype	Assembly technique	Readout technology	spatial resol (phi × Rphi)	Low mass	Dead area from support frames	Dead area in active area	FE cards connection
FIT FT-GEM 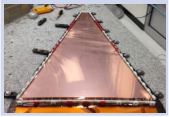	Assembled – Technical issues – Fixes underway X	**Mech. Stretching technique - chamber can be reopened √**	1D Zigzag strips X	100 µm √ **but 1D only**	**Yes √**	Carbon Fiber, G10 Fiber glass, metallic piece X	**No spacers √**	Standard - Outside active area √
UVa FT-GEM 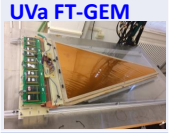	**Assembled – Tested in beam at FNAL √**	Glued frames - chamber can't be reopened X	**2D U-V stereo-angle strips √**	100 µm × 400 µm √	**Yes √**	**Fiber glass (G10) 15 mm √**	300 µm straight spacers grid X	**Zebra - Outside active area √**
TU FT-GEM 	STAR FGT Technical issues – Fixes underway X	Glued frames - chamber can't be reopened X	**2D radial-Azimuth strips √**	**100 µm × 100 µm √**	**Yes √**	(G10) 15 mm but FE cards on the side X	50 µm Kapton rings X	Outside active area But FE on side X ?

Figure 25: Comparisons of the differences in assembly techniques and readout strip layer options of the three large GEM prototypes designed at UVa, FIT and TU as R&D for the forward tracker of an EIC detector.

development of large area and low mass triple-GEMs in order to minimize the impact of multiple scattering on the angular and momentum resolution and the dead area affecting the overall efficiency of the detectors. Each of the prototypes proposed by the three institutes is expected to meet these detector requirements for EIC tracking system. However there are some key technical differences between the prototypes proposed by the three institutes in the area of the assembly technique of the detector and the choice of the readout strip layer approach to reach the performances spatial resolution imposed by the EIC detector requirements. The table shown in Fig.25 provides a brief summary of the main characteristics of each of the prototypes and the impact of the technological choice on the expected performances of the detectors.

The large GEM prototype from the FIT group adopted the mechanical stretching technique developed for the CMS GEM (LHC CERN) which ensures that large-area triple-GEM could be assembled with no spacer grid, eliminating the dead area and low efficiency create by spacers in the active area of the chambers. This technique also allow the detectors to be re-opened if there is a need to replace faulty parts (GEM foils or readout layer etc...) during the assembly or operation of the detectors. However, the cost for this assembly technique is the need of wider and heavier material (including metallic screws and pieces) for the support frames to sustain the tension of the stretched GEM foils readout layer and drift cathode foils. This will increase the dead area and multiple scattering in localized region of the active area of the detectors when large trapezoidal GEM modules are assembled in the disk configuration of the EIC forward tracker.

By contrast, the prototype constructed at UVa is based on the more traditional assembly techniques where the stack of support frames with the stretched GEMs foils are glued together during the assembly. In this configuration, a grid of very thin (300 μm) spacers are required in the active area between each GEM layer in the stack to ensure that a uniform gap between layers of the stack is maintained. The presence of spacer grids amounts to a small, $\sim 1\%$, dead area in the active area of the detector and might also slightly complicate the tracking during reconstruction. However, the main advantage of this assembly technique is that it allows to minimise the overall dead area and limits the degradation of the detector spatial resolution due to multiple scattering of the detector in a disk configuration because the material for the GEM support frames is significantly lighter and smaller in size.

The TU prototype, which adopted similar assembly technique, is experimenting with thin kapton rings as a replacement of the spacer grid in order to reduce the fabrication and assembly cost. However, the benefit of Kapton rings over spacer grids remains to be demonstrated.

In addition to the different assembly techniques, the choice of readout strip layer technology is also different

for each of the three prototypes and is an area of sustained R&D. The FIT group has developed the zigzag strip readout technique which is expected to provide 1D spatial resolution performance of $\sim 100\mu$m in the azimuthal direction with a significantly low number of electronic channels to be read out. However, zigzag readout, in its current stage of development, only truly offer a one dimensional information of the particle position while the U-V stereo-angle strip readout under test at the UVa and the radial-azimuthal readout proposed by TU group will offer excellent 2D spatial resolution in both radial and azimuthal direction, but with twice more electronic channels to be read out. The spatial resolution expected for the U-V strips readout for UVa prototype or the radial-azimuthal strips readout for the TU prototype team will easily meet the requirements for an EIC forward tracking detectors with better than than 100μm in the azimuthal direction and 300μm in the radial direction for both detectors. The pros and cons of each of the technologies is summarized in the table of Fig. 25.

2.2.1 What was planned for this period?

2.2.1.1 Florida Tech Large Carbon Fiber GEM Prototype with zigzag readout

The goal for the last funding period was to assemble and operate the refurbished low-mass prototype and to characterize its performance, e.g. gain curves, with X-rays at FIT. On the simulation side, we planned to continue to reach out to EICroot tracking experts so we can study track-hit residuals as a function of forward tracker material.

2.2.1.2 UVa Large GEM Prototype with 2D U-V readout

For the current cycle, we planned to:

1. **Characterisation of large EIC GEM prototype:** Test different types of zebra strips with UVa large GEM prototype to investigate the source of the distortion of the detector signal and its impact on the poor and non uniform spatial resolution performances that we observed from FNAL 2018 test beam data.
2. **Acquisition of the VMM-SRS electronics:** See relevant paragraph in section 2.1.2.5.

2.2.2 What was achieved?

2.2.2.1 Florida Tech Large Carbon Fiber GEM Prototype with zigzag readout

Refurbishment of low-mass EIC Forward Tracker GEM detector prototype: We continue to struggle with shorts between adjacent foils in the Triple-GEM stack of this large prototype detector. With the detector mounted on a frame as shown in the previous report, an attempt to remove shorts by clamping the carbon fiber frame of the detector to the rigid support structure was not successful. The detector would hold HV only up to $V_{drift} = 2$ kV and spark above that value. A voltage of $V_{drift} = 4.2$ kV is needed to operate the detector. Consequently, we removed the detector from the frame, opened it again in the cleanroom, and disassembled the foil stack. A campaign to pre-stretch every single foil with tape during stack re-assembly, including pre-stretching the readout foil, before applying final tension with the stretching screws did not succeed, either. Afterwards, we observed a persistent short across the 2 mm induction gap. We enlisted help from our colleagues at Temple who graciously provided us with their spare 2 mm tall kapton rings from their earlier FGT assembly. We used these to partially fill the induction gap to maintain the gap distance (Fig. 26). Due to the limited number of available rings, the gap could not be completely filled, though. We are aware that the rings might move around slightly during handling, but we would expect that they stay in position once the chamber is not being touched anymore during operation. At the time of writing this report, the stack is re-assembled, but not stretched, yet.

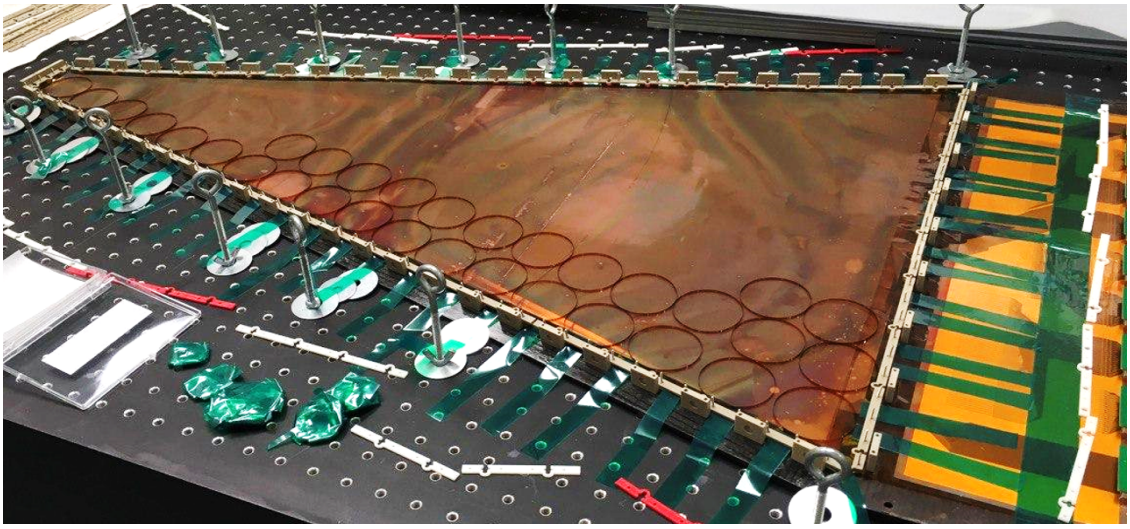

Figure 26: Large low-mass GEM detector with kapton rings placed as spacers in the induction gap. Green tape for pre-stretching the readout foil is also visible.

For general reference, we have done an accounting of the material in the detector prototype not only in the active region, but also in the chamber periphery where the mechanical support structure is located. The results are listed in Tab. 1. While material across the entire active area accounts for less than one percent of a radiation length, the material a particle would encounter when traversing the detector periphery varies from around 60% of a radiation length in most locations up to 139% in the worst case if the particle were to traverse the full length of a GEM stack screw.

Table 1: Material for EIC Forward Tracker GEM detector prototype with carbon fiber (CF) frames.

Location in detector	**Rad. Length X/X_0**	**Comment**
Active area	0.84%	Triple-GEM stack and gas windows
Border of GEM stack with inner frames		
best case	60.3%	track going only through inner frames
worst case	139.4%	track hitting full length of a GEM stack screw
Pull-out location		
best case	61.6%	track hitting only pull-out and CF frames
worst case	111.8%	track going through CF frame closing screws
Outer gas frame location		
best case	64.6%	track hitting only outer gas frame and CF frames
worst case	87.0%	track hitting gas inlet or outlet
Edge of carbon fiber support frames	56.4%	

2.2.2.2 Study of the issue with drift cathode foil collapse of UVa large GEM Prototype

These past few months, we took a look at an issue with the large GEM prototype that we have been repeatedly confronted with when operating the prototype in 2018 test beam at FNAL and later with x-ray source at UVa. We observed that when operating the detector in FNAL beam or x-ray source where the particle flux is a few order of magnitude higher than the cosmic rate, after a while, the detector's drift cathode foil will collapse onto the detector's entrance window foil and the two foils will stick together. This results to a deformation of the drift volume as illustrated by the right cartoon of Fig. 27. The wrinkles observed on the pictures show the boundary between the inner area where both foils are glued to each other

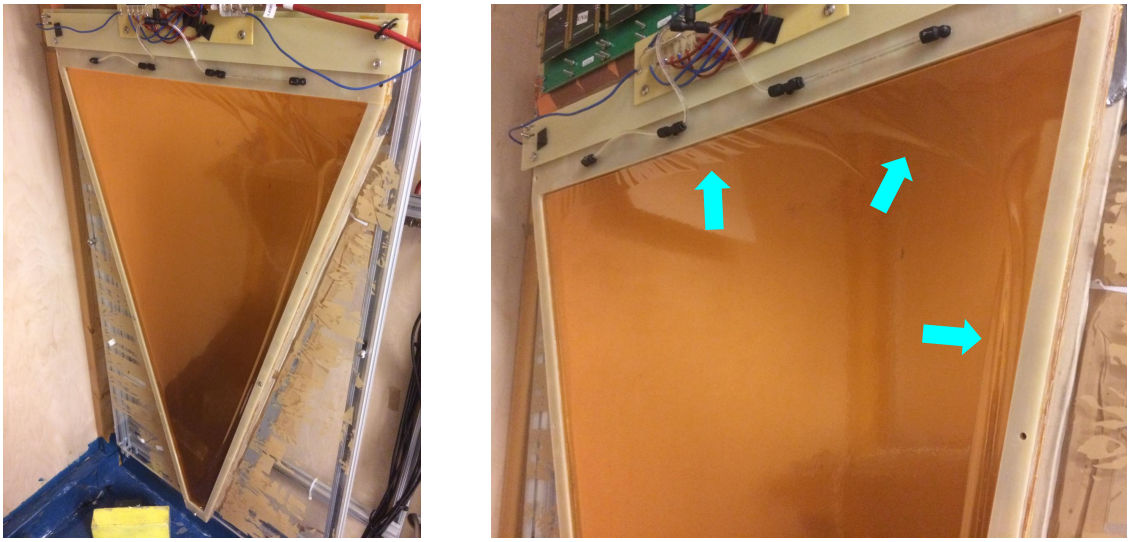

Figure 27: The collapse of the cathode foil onto the entrance window foil is clearly visible with the apparition of wrinkles (see cyan arrows) on the edge of the detector after exposure to high flux of x-ray source.

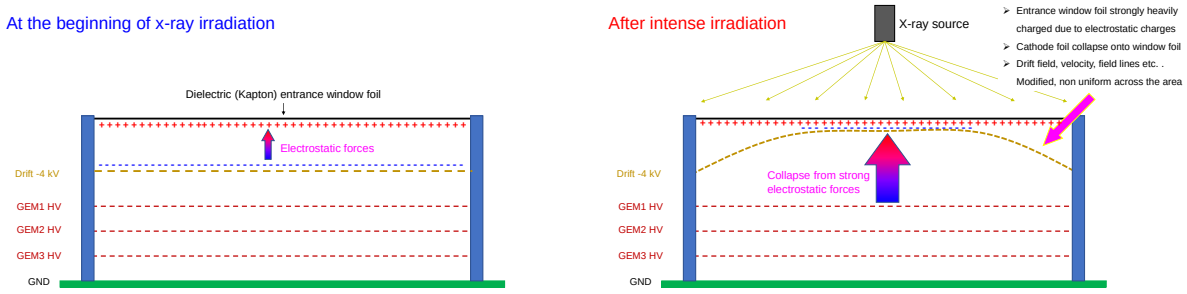

Figure 28: Hypothesis. *left:* Cross section view at the beginning of the exposure to high flux x-ray; *right:*, after a few days of exposure. The cathode foil collapse onto the entrance window.

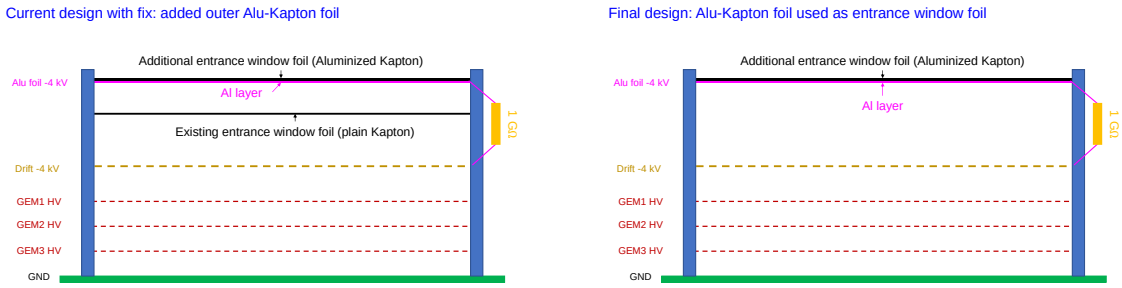

Figure 29: *left:* Cartoon view of the prototype with the fix to the drift cathode collapse issue; *left:* Permanent fix to the collapse issue for future large GEM with the plain Kapton foil entrance window replaced by Al-Kapton foil maintained at the same voltage as the drift cathode.

and the remaining area in the peripheral where, because of the mechanical constraints of the support frame, the foils can not stick together. We think that the problem is caused by electrostatic charging up of the ions and electrons from the ionisation of the Ar-CO2 molecules inside the volume between the entrance window foil and the drift cathode. In our hypothesis, when the particle flux to the detector is high , the charging up lead to the accumulation of ions and electrons on either side of the dielectric foils. The dry Ar-CO2

gas in the detector prevent a conductive pathway to the charges to recombine or flow to the ground and therefore, the electrostatic force caused by the accumulated charges on the foil becomes strong enough to trigger th foils to collapse onto each other as we illustrate on the cartoons of Fig. 28. The effect usually starts from a small area and then progressively expands to a larger area (up to 90% of the total active area) as the detector exposure to high particle flux continues. Once the foils collapse, there is no easy and obvious way to revert to the initial state other than blowing moisturised gas inside the chamber to flush out the electrostatic charges. This approach works to some extend as a temporary fix, and is a confirmation to our hypothesis that electrostatic charge accumulation causes the foils to collapse, but as soon as the detector is exposed again to high particle flux, the collapse will take place again. Moreover, blowing moisturized gas into a triple-GEM detector is not only a practical way to address the problem, it is also a dangerous practice because the detector need to operate in a dry environment to prevent aging and discharge. We proposed a more permanent fix to the problem of collapse of the drift cathode foil of our large prototype, which consists on stacking one framed Al-Kapton foil on top of the entrance window foil, separating by a 3 mm support frame. The conductive (Al) side is facing the entrance window foil and is maintained at the same voltage as the drift cathode (typically 4 kV) as shown on the left cartoon of Fig. 29. In this configuration the initial entrance window Kapton foil is now sandwiched between the drift cathode and the added Al-Kapton foil creating a Faraday cage and therefore preventing the charging of entrance window foil.
We implemented the fix described above to the large GEM prototype and extensively tested in high intensity x-ray for several consecutive weeks to validate our hypothesis. Fig. 30 shows the experimental setup with on the right picture, the prototype in the x-ray box at UVa for the continuous exposure to high rate particles and on the left, the setup for cosmic data run with two trigger scintillator PMT detectors in coincidence. This trigger detectors cover just a limited area of the prototype. Preliminary data analysis from both x-ray and cosmic runs taken intermittently during x-ray irradiation, shows that the problem with drift cathode foil collapsing onto the entrance window foil disappear with the fix that we implemented. This is also a clear demonstration that our hypothesis for the reason of the collapse is the right one. Fig. 31 show the 2D hit map of reconstructed positions of cosmic data before (top right) and after (bottom right) the fix was applied. This measurement were performed after the prototype had been continuously exposed to x-ray data for a several days. The detector coverage area by the cosmic events (the red polygon on the pictures) is limited by the acceptance of the trigger scintillators paddles. For the cosmic runs, 4.1 kV was applied to the

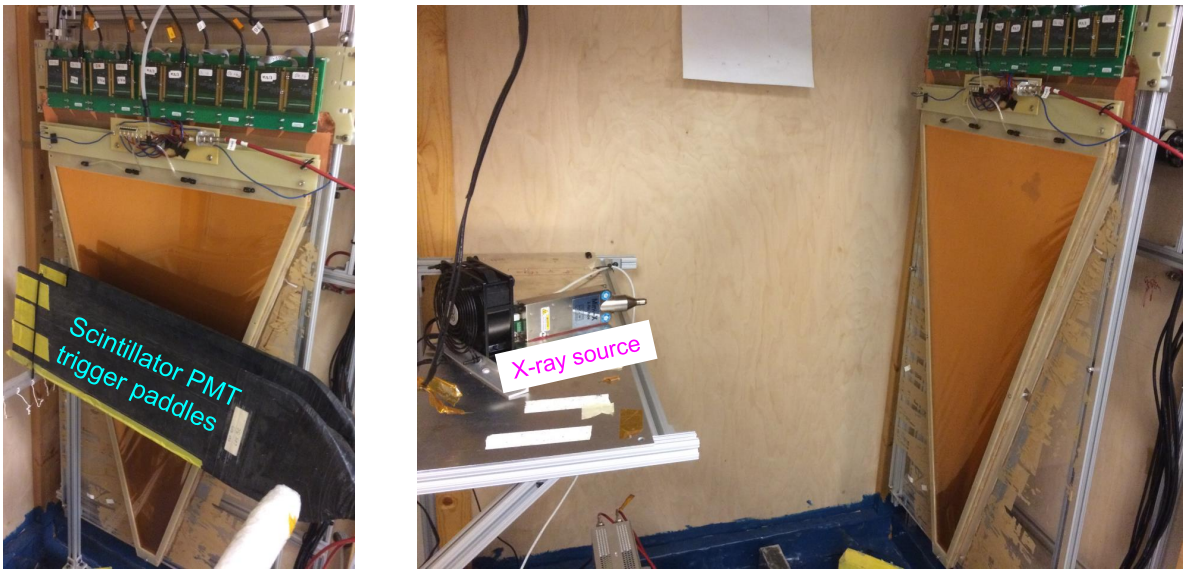

Figure 30: Experimental setup for the study of drift cathode collapse effect: *Left:* Setup for cosmic tests after exposure to x-ray; *left:* Setup for lengthy exposure to high intensity (high particle flux) x-ray.

prototype HV divider, which is standard voltage for a triple-GEM to operate in fully efficient mode. On the left plot of Fig. 31 corresponding to cosmic reconstructed hit map, after x-ray exposure but before the fix was implemented, the efficiency to cosmic was extremely low. This is similar to a situation where the electric

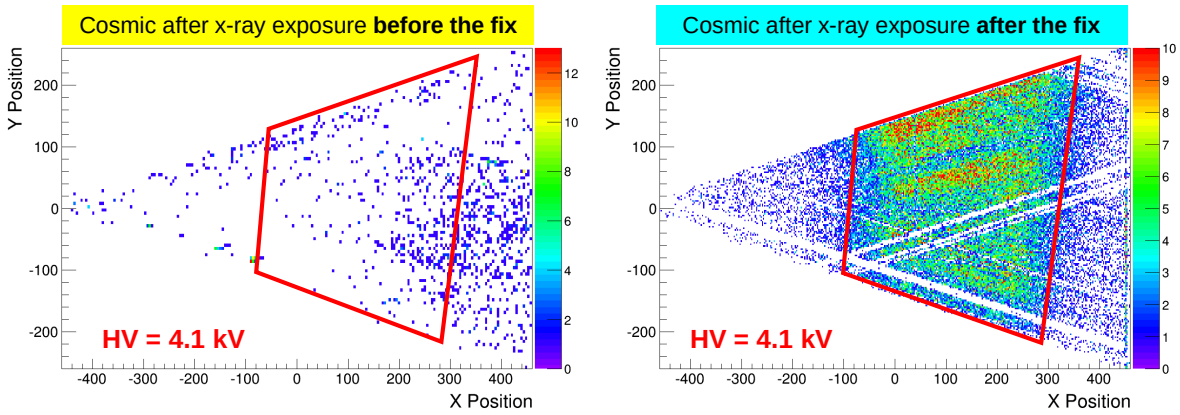

Figure 31: Cosmic data: *Left:* Hit map before the fix was applied, showing evidence of partial collapse of the drift cathode foil during x-ray exposure; *Right:* Hit map after the fix, No drift foil collapse were observed from the data.

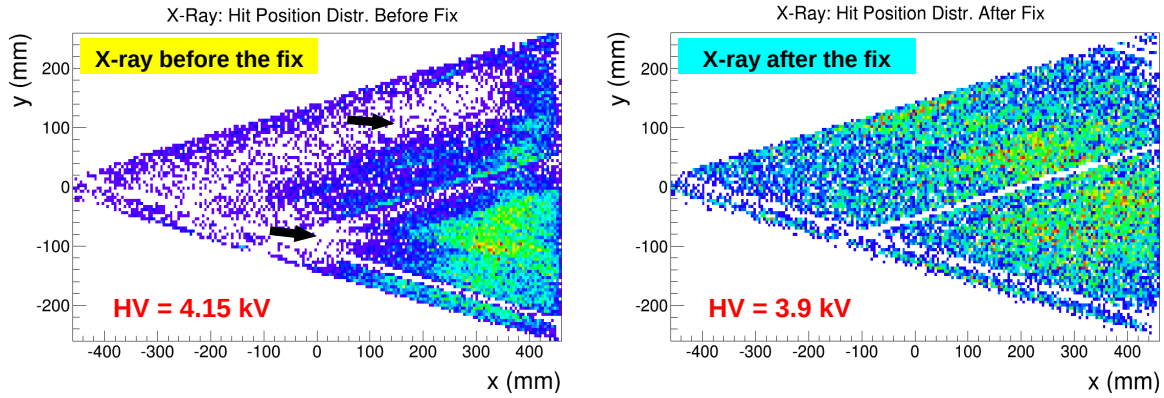

Figure 32: X-ray data: *Left:* Hit map before the fix was applied showing evidence of the drift cathode foil collapse (black arrow); *right:* Hit map after the fix, with no evidence of drift cathode collapse..

field in the drift region of the detector is almost equal to zero, or too low preventing ionization charges to reach the holes of the first GEM amplification stage. This can be explained by the deformation of the drift cathode foil when it collapses to the entrance window. The electric field is considerably reduced because the drift gap increases by a factor 3 or more. After the fix is implemented, the detector efficiency performances is restored as shown on the right plot of Fig. 31 with the area inside the trigger acceptance (red trapezoid) is densely populated with cosmic events as expected for a fully efficient detector. With the additional Al-Kapton layer glued to the chamber, we no longer can visually see if the drift cathode foil actually collapses onto the entrance window foil, but from the data and the restored performances of the chamber, we can demonstrate that the problem has been fixed or at least drastically reduced. Similar observations were made with x-ray data taken intermittently during the long and continuous exposure of the chamber to high flux x-ray. Fig. 32 shows the hit map from the reconstructed x-ray before and after the fix was implemented. On the left plot, before the fix, once can see a large area of the detector with very low efficiency (see black arrows) even when a voltage as high as 4.15 kV was applied to the HV divider to increase the detector gain. In normal conditions, standard triple GEM detector is fully efficient for converted x-ray photons at a voltage of 3.9 kV on its H divider. This is what we observed on the hit map plot on the right of Fig. 32 after we had the fix in place. The effect is also seen on the 2D spatial distribution of the average ADC as shown in the plots of Fig. 33. Average ADC distribution plots such as these ones represent a quick qualitative measurement of the detector gain uniformity across its active area.

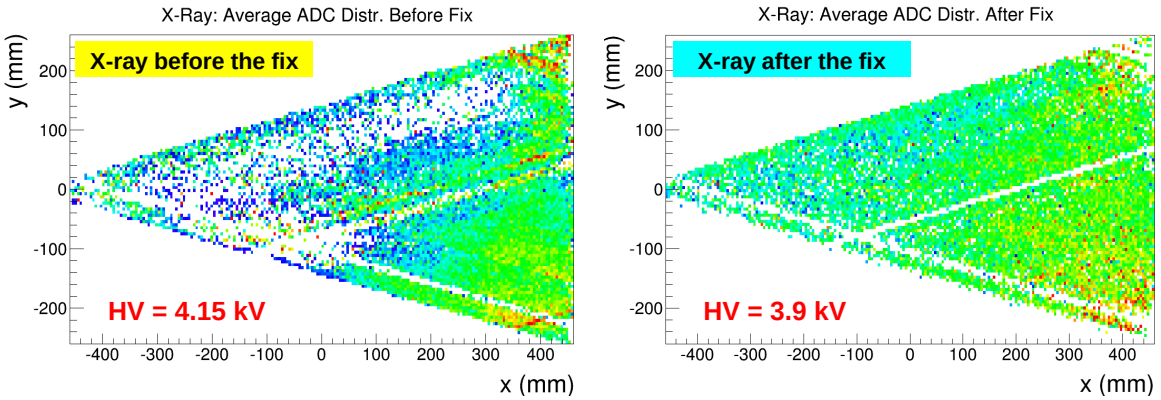

Figure 33: X-ray data: *Top left: Left:* 2D distribution of the average ADC (gain uniformity) before the fix; *right:* 2D distribution of the average ADC (gain uniformity) data after the fix.

From the lessons learned with the large GEM prototype built at UVa for EIC Forward Tracking detector R&D, we would recommend for the future that for large area and low mass triple-GEM detectors, one uses directly aluminized Kapton with the Aluminum side (conductive side of the layer) facing inward and biased at the same voltage than the drift cathode, as illustrated on the right cartoon of Fig. 29) to prevent any type of charging up due to electrostatic effect. This would allow to avoid adding the additional layer to prevent the collapse as we did for our prototype because it was not possible for us to replace the plain Kapton foil initially used as entrance window with the Al-Kapton foil since the detector frames are glued together during the assembly.

2.2.3 What was not achieved, why not and what will be done to correct?

2.2.3.1 Florida Tech Large Carbon Fiber GEM Prototype with zigzag readout

On the hardware side, the refurbishing of the detector is still ongoing so that we have not yet been able to commission the detector. On the simulation side, we are still struggling with extracting information on track positions from EICroot to calculate residuals as function of detector material. This is due to the complexity of the EICroot track fitting code, inexperience of our undergraduates, lack of in-house post-doctoral support from the project, and limited availability of EICroot experts.

2.2.3.2 UVa Large GEM Prototype with 2D U-V readout

We have not yet procure the different types of zebra strips sets to test on the large GEM prototype and study the impact of the zebra strips quality on the performances of the detector. For this part of R&D, we concentrated on fixing the problem related to the collapse of the drift cathode foil as we reported in the section 2.2.2.2.

2.2.4 What is planned for the next funding cycle and beyond?

2.2.4.1 Florida Tech Large Carbon Fiber GEM Prototype with zigzag readout

We will check if the detector can hold HV after inserting the Kapton rings into the induction gap. If yes, we plan to perform quality control tests on the refurbished low-mass prototype and to characterize its performance, e.g. gain curves, with X-rays at FIT.

2.2.4.2 UVa Large GEM Prototype with 2D U-V readout

For the coming cycle of FY20 and beyond, we plan to acquire different types of zebra strips and test them with the large EIC GEM prototype. We strongly suspect the type of zebra strips that we are currently using for the prototype, to be the main source of poor signal quality resulting in a spatial resolution that we obtained from the FNAL test beam data far worse than expected. We will procure the different types of zebra strips and instrument the prototype with for test in x-ray and cosmics.

3 RICH Particle ID

3.1 Hybrid MPGD for RICH - INFN Trieste

3.1.1 What was planned for this period?

3.1.1.1 MPGD sensors of single photons at INFN Trieste

The activity foreseen for the year 2019 includes the completion of the analysis of the data collected at the 2018 test beam exercise where a first version of the prototype was studied.
The realization and characterization by laboratory tests of a second version of the prototype is also foreseen. The construction of this second version of the prototype is related to the observed non-uniformity of the gain. A modified version has already been designed. The construction and characterization of the modified prototype will take place in 2019.

Corresponding **milestone for 2019**:
September 2019: The completion of the laboratory characterization of the second version of the photon detector with miniaturized pad-size.

3.1.1.2 New Photocathode Materials development at INFN Trieste

The activity foreseen for the year 2019 is related to the status of the R&D. The initial studies to understand the compatibility of a photocathode based on NanoDiamond (ND) particles with the operation in gaseous detectors and, in particular, in MPGD-based photon detectors, have been performed in 2018. The characterization of THGEMs with ND coating, both in the case of hydrogenated and non-hydrogenated powder has presented unexpected features, even if very different in the two cases. The foreseen activity consists in further laboratory studies to explore these performance in order to understand the origin of the modified THGEM behavior by producing under controlled parameters a new set of small-size THGEMs, that then will be fully characterized.

Following the activity planning, the **milestone for 2019** is:
September 2019: The completion of the studies to understand the performance of THGEMs with ND coating, both in the hydrogenized and non-hydrogenized versions.

3.1.2 What was achieved?

3.1.2.1 MPGD sensors of single photons at INFN Trieste

The activity of the period January-June 2019 is reported. The activity has partially deviated from the planning. This deviation has been suggested by the ongoing analysis of the test beam data and the further laboratory studies of the prototype, as discussed in the following.

The main results that could be extracted from the test beam and laboratory exercises have been already presented in the previous report (July 2019 eRD6 progress report): the good electrical stability of the detector, the high gain achieved in stable conditions, the fine time resolution, the capability to operate in pure methane atmosphere. Nevertheless, the noise figures, already extensively discussed in the previous report, prevent from accessing other important detector features. The typical noise level is at 3300 electrons equivalent, while the detector gain is about 30k. This results, applying the typical 3-σ(noise) threshold, in a photoelectron detection efficiency of approximately 70%. Moreover, whenever the physical signal is collected in more than one single pad, the probability to lose part or the whole of it, is high because of the threshold cut. The small cluster size reported in the previous report is certainly related to this feature. As already reported, the relatively high noise level is due to several features: the intrinsic noise introduced by the SRS implementation in the configuration used by us, the need of an adapter card and noise related to the arrangement of the boards equipping the prototype. Concerning the last source of noise, the cards with resistors supplying the HV to the individual pads and the read-out adapter cards hosting the SRS-APV25 cards are parallel with small distance between them (Fig. 34). We do not regard the present noise figure as an intrinsic limitation of the detector architecture. In fact, the novel photon detectors installed on the COMPASS RICH detector, which have a hybrid MPGD architecture as well, and are read-out by APV25 FE chips [18], exhibit a typical noise level lower than 900 electrons equivalent [8]. Nevertheless, the present noise level prevents us from obtaining a complete characterization of the proposed detector architecture and accessing key aspects of its ultimate performance. The considerations presented above suggest to give priority to activities dedicated to control and reduce the noise level presently affecting the studies of the prototype. Two different actions have been decided and started. They are presented in the following.

The design of the second version of the prototype has been modified with the goal of minimizing the noise. Two main modifications are implemented. The resistor card is eliminated and the resistors, SMD ones, are directly mounted onto the anode PCB. Therefore, the pickup noise from the resistor cards, that are distributing HV, to the SRS-APV25 cards is eliminated; moreover, more physical space becomes available around the SRS-APV25 cards, making a more robust grounding of each individual card possible. The second modification is related to the careful track routing in the anode PCB. The anode PCB a crucial element of the detector: the resistive micromegas by descrete elements, which is the last amplification stage in our PD architecture, is implemented here (Fig. 35 (a), (b) and (c)). In the first version of the anode PCB the signal tracks from the signal collection pads (embedded in the PCB) do not have the same length. They are, also, running over the pads themselves, even if in PCB layers different from the one hosting the pads. Therefore, non negligible and different parasitic capacitance is affecting the signal lines. This is another source of noise pickup and, moreover, it affects the amplitude of the signals from the different pads modifying the effective pad gain (Fig. 35 (d)). We are confident that the improved version will result in a lower noise level offering the opportunity to better understand the performance of our approach to gaseous PD for EIC, even if not yet the ultimate performance. This because the APV25 implementation in the SRS system is not designed in order to optimize noise figures. The track routing designed for the second version is completely revisited and performed accounting to the following prescriptions:

- providing HV distribution via SMD resistors directly mounted on the PCB; each resistor is mounted over its pad;
- making vias vertical in order to minimize crossing signal lines;
- improving the equalization of the signal line length in order to have the same input capacitance, therefore avoiding different effective pad gains.

The novel design is illustrated in Fig. 36.

The second line of activity concerns the FE electronics to be coupled to our detector.

A novel chip designed for MPGD application and, in particular, for the New Small Wheel (NSW) upgrade project in ATLAS is VMM3 [19, 20, 21], developed at Brookhaven National Laboratory and fabricated in the 130 nm Global Foundries 8RF-DM process. Its main characteristics are [22]: 64 channels, highly configurable parameters, the capability to handle signals of opposite polarities, high range of input capacitance, low-noise

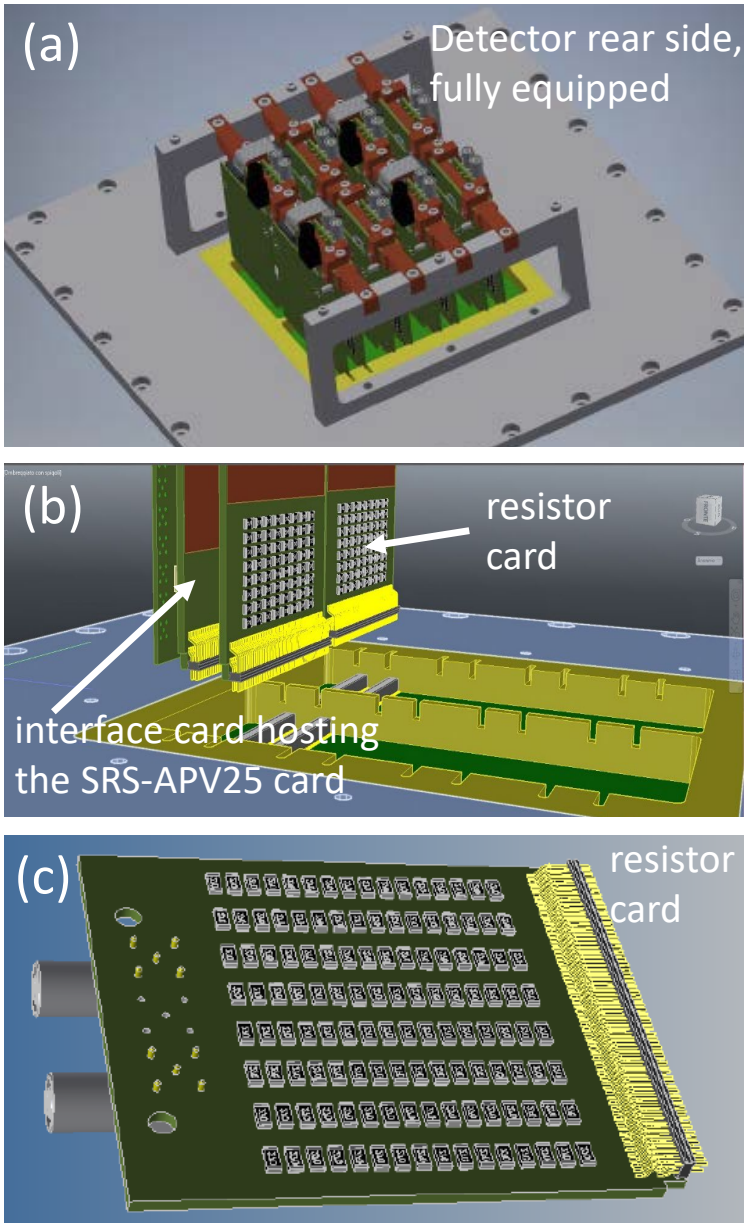

Figure 34: Prototype design (from the January 2018 eRD6 progress report). (a) The rear side of the detector fully equipped. (b) Detector rear side: detail of the connectors, the resistor cards and the interface card hosting the SRS-APV25 card. (c) The design of the resistor card.

charge amplifier with adaptive feed-back, a shaper with baseline stabilizer, a discriminator with trimmer, a peak detector, a time detector and low power consumption. Other features of major interest are a dedicated digital output for Time-over-Threshold (ToT) or Time-to-Peak (TtP) to be performed by external TDCs, three analogue outputs for peak detector, time measurements, monitoring output, a pulser for test options, the real time access to the data output. These outputs are continuously running with only 250 ns dead-time per channel or in triggered mode. Amplitude measurement with 10 bit resolution and time stamp with 20-bit resolution are externally possible. Al least three of the above mentioned features are of great interest for us, namely (i) the low noise figure, (ii) the capability to effective coupling with detectors in a wide capacity range and the (iii) architecture designed for trigger-less operation. Characteristics (i) and (ii) are specifically

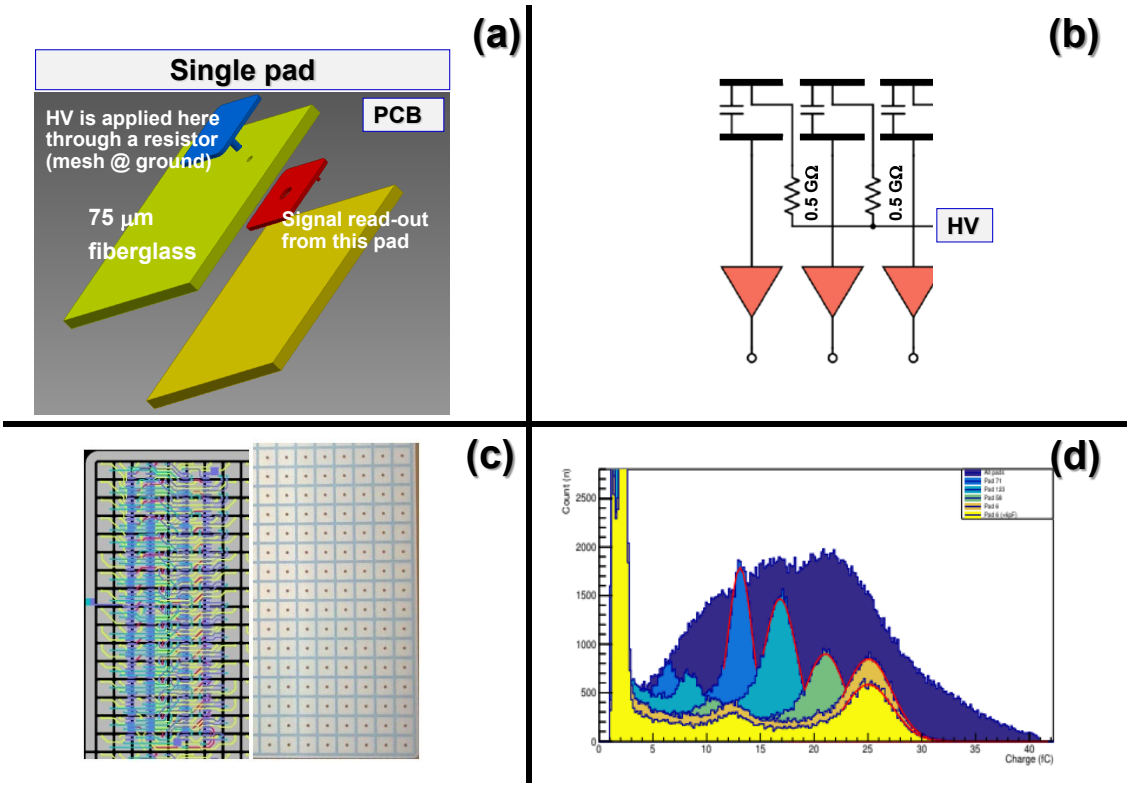

Figure 35: The resistive micromegas by discrete elements((a) and (b) are from the June 2016 eRD6 progress report; (d) is from the June 2018 eRD6 progress report). (a) The principle is illustrated by a single pad; the different layer of the PCB forming the micromegas anode are schematically shown: the blue pad is the anode electrode of the micromegas kept at positive voltage; it directly faces the micromesh; the red pad is embedded in the PCB and the signal is transferred from the blue to the red pad by capacitive coupling. (b) The principle is illustrated by the electrical scheme: the top elements of the capacitors are the pad forming the micromegas anode (blue pad in (a)), the bottom elements of the capacitors (red pad in (a)) are connected to the Front-End (FE) electronics. (c) The first version of the anode PCB. (d) ^{55}Fe amplitude spectra collected by different pads with the first version of the prototype.

beneficial to our single photon detection application, namely an application requiring single photoelectron detection, performed by a hybrid MPGD where the last multiplication stage is by a micromegas, namely a relatively high capacitance detector. These characteristics are presented in Fig. 37, where also the APV25 characteristics are shown, for comparison. Feature (iii) makes the VMM3 ASIC suitable for modern trigger-less read-out architectures, therefore offering the advantage that VMM3 can be regarded, from this point of view, as a valid FE candidate for EIC detectors.

VMM3 is being implemented in the SRS system, nevertheless the optimization of the noise figure is not a primary goal in this implementation. Therefore, the use of VMM3 in SRS implementation is not of interest for our application.

The stand-alone VMM read-out board MMFE1 (Fig. 38) has been developed in the context of the ATLAS NSW project. It has been design to exploit all the most relevant VMM3 features, including the good noise figures. It houses two VMM3 chips for the readout of 128 channels. This stand-alone board offers an opportunity to understand if the VMM3 FE chip is valid solution for the read-out of our gaseous PDs. Of course, it not adequate for an extended read-out system. In case VMM3 coupled to our gaseous PD offers promising performance, the major effort of a complete read-out system exploiting the VMM3 features on the scale of an extended system, have to be addressed in the future, in a collaborative effort with other potential

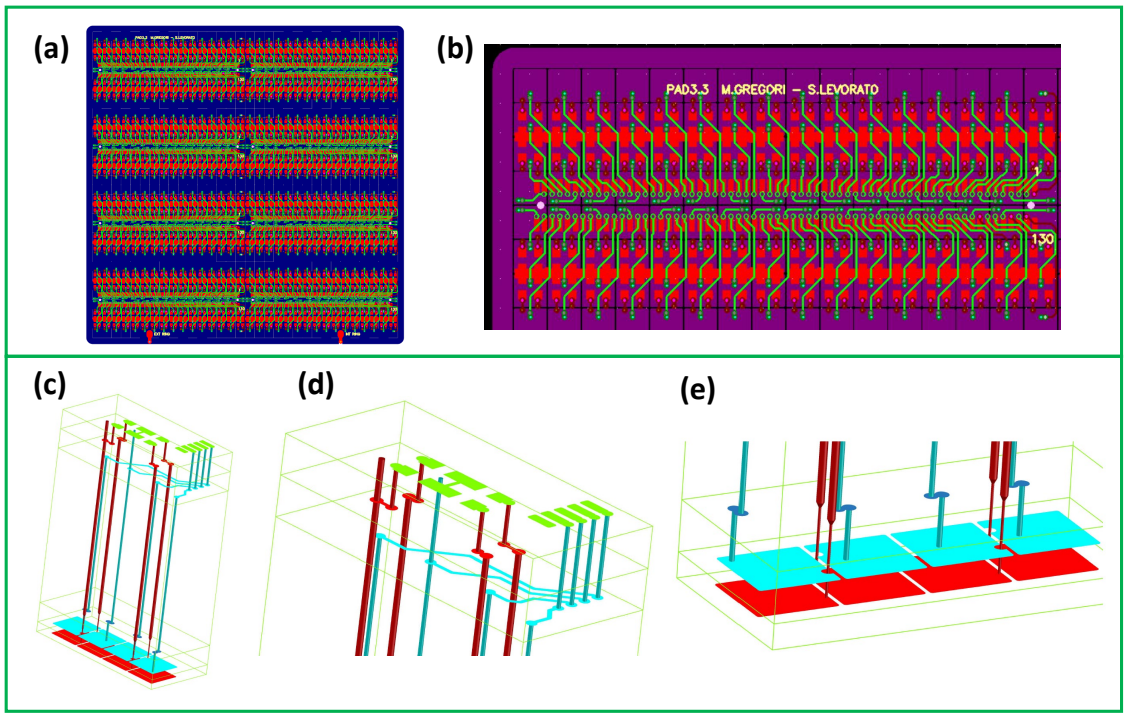

Figure 36: Design of the PCB for the resistive micromegas, improved version. (a) Connector face. (b) Zoomed view of a portion of the connector face; the pads for the SMD resistors are visible. (c) The vertical vias. (d) Zoomed view of a portion of the vertical vias at the connector face. (e) Zoomed view of a portion of the vertical vias at the pad face, facing the micromegas micro mesh.

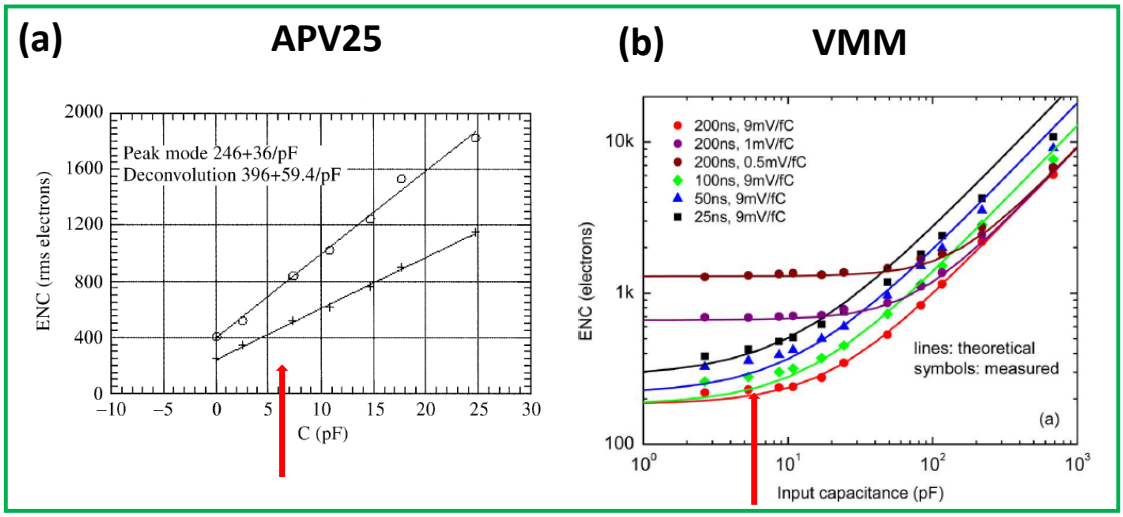

Figure 37: Equivalent noise charge as a function of the input load capacitance; (a) APV25 [23]; (b) VMM [19]. The red arrows mark the capacitance load of our prototype with 3×3 mm^2 pads.

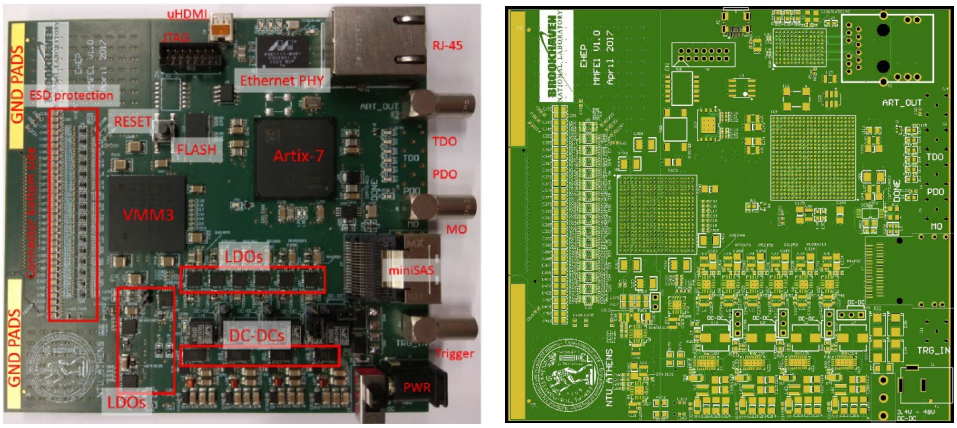

Figure 38: Picture of a MMFE1 board.

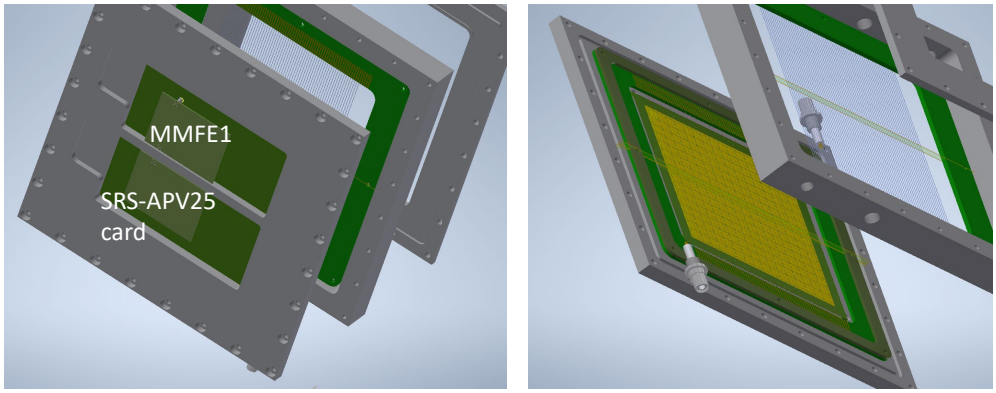

Figure 39: Principle design of the dedicated prototype micromegas for comparative studies of detector readout via VMM3 implemented in the MMFE1 board and via APV25 implemented in the SRS-APV25 board.

users.

Two MMFE1 boards are presently being produced for our tests. We are going to use a MMFE1 board to read out part of a dedicated micromegas prototype (Fig. 39), designed according to our architecture of resistive micromegas changing the connectors so that part of the detector can be read with the MMFE1 board and part using an SRS-APV25 card. The dedicated prototype is optimized to allow comparative testing of the two read-out options. The PCB for the anode of this dedicated prototype is presently being design.

In conclusion, in spite of some deviation from the original work planning, work has progressed preparing two different approaches to reduce the noise level in the present prototype setup. This includes the design, now completed, of the second version of the prototype and the explorative study of coupling a different FE chip, namley VMM3, to the proprotype. The work reported above also suggests the next steps, which are presented in Sec. 3.1.4.1.

Table 2: *New samples of HND coated substrates used for the 2019 studies.*

substrate type	sample label	coating material	number of spray shots
THGEM	TB IX	ND	300
THGEM	TB VIII	HND	140
THGEM	TB III	HND	43
THGEM	TB VII	HND	55
THGEM	TB XIX	HND	59
THGEM	TB XI	HND	250
disc	PBC1	ND	100
disc	PBC2	ND	100
disc	PBC3	ND	200
disc	PBC4	ND	200
disc	PBC5	ND	50
disc	PBC6	HND	50
disc	PBC9	HND	25
disc	PBC7	HND	50
disc	PBC10	HND	100
disc	PBC11	HND	200
disc	PBC8	HND	400

3.1.2.2 New Photocathode Materials development at INFN Trieste

The effort to understand the performance features of Hydrogenated NanoDiamond (HND) photocathodes and their coupling to THGEMs has progressed by laboratory studies, along different lines, as reported in the following. These studies required the realization of a new set of THGEMs, as well as of disks by metallized fiberglass, 1 inch diameter. THGEM geometrical parameters are our standard ones, namely: 0.4 mm thickness, 0.4 mm hole diameter, 0.8 mm hole pitch, no rim and 30×30 mm^2 active surface. These different substrates have been coated with either ND or HND films. Coating is by the spray technique, developed in Bari and already described in previous reports. Coating applying different numbers of spray shots have been realized in order to understand the relevance of this parameter. A summary of the samples realized and studied is presented in Table 2.

In 2018, it was observed that the breakdown voltage of THGEM coated with HND powder is at voltages too low respect to what required in stable photon detectors, while HND coated THGEMs are of major interest because of the high Quantum Efficiency (QE) of the HND converter. A possible cause of the reduced electrical rigidity is related to the NDH most likely present also inside the THGEM holes after a coating process. An attempt to overcome this difficulty is based on THGEMs formed by two layers, each one of thickness one half that of the final THGEM, and where only one of the faces is Cu-coated. The two layers are assembled together keeping externally the metallized faces, while one of the two layer is coated before assembling the final THGEM. Half-THGEMs have been produced and coupled to form a single THGEM. Very relevant gain evolution versus time has been observed during preliminary exercises performed to characterize these novel devices (Fig. 40): these effects are related to the residual hole misalignment, which is playing a role more relevant than expected. This approach has been suspended.

A different attempt to increase the electrical rigidity of HND-coated THGEMs has been tried. Hydrogenated materials are hygroscopic. A heat treatment of HND-coated THGEMs has been applied in order to remove the surface humidity: the coated THGEM is kept in oven for 24 h at 120^o C degrees. The THGEM electrical rigidity has been fully recovered (Fig. 41). The stability of the electrical rigidity recovery has been verified repeating, approximately one month later, the gain measurement. The effect of the heat treatment on the

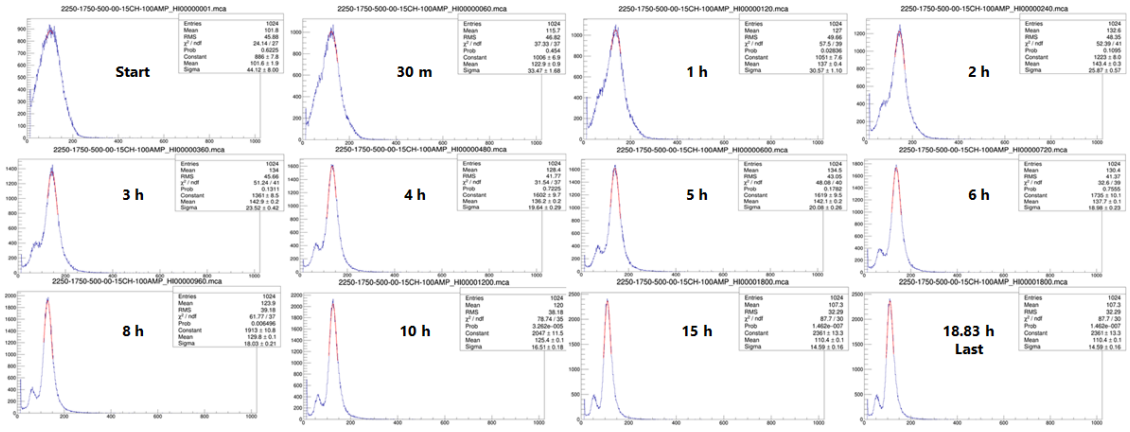

Figure 40: The time-evolution of the amplitude spectra collected illuminating the THGEM formed by two half THGEM layers with X-rays from a ^{55}Fe source.

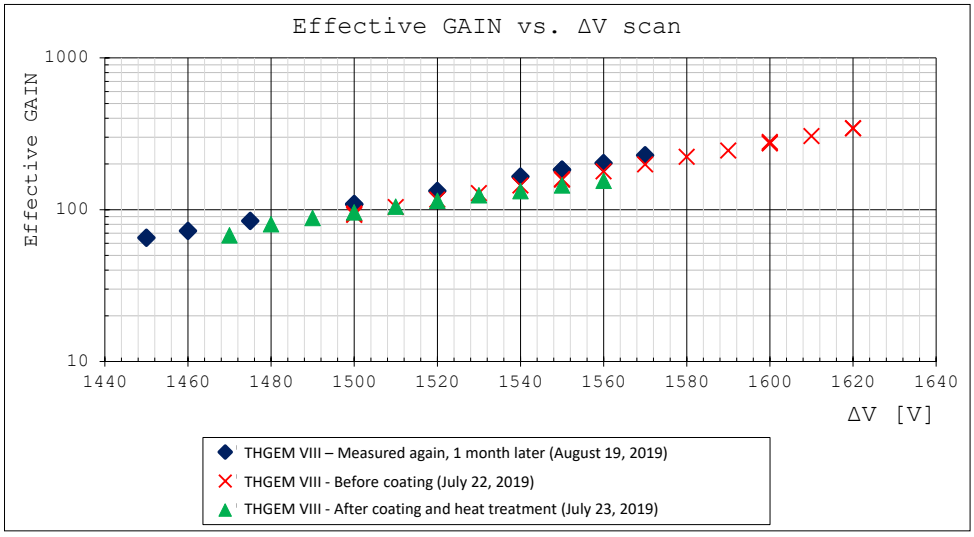

Figure 41: Effective gain versus applied biasing voltage for a same THGEM measured for the bare device and with HND coating after applying the heat treatment; the measurement has also been repeated a month later.

QE has been studied making use of the setup available in Bari [24], where only small-size samples can be studied. Therefore, the disk samples have been used. The QE measured after the heat treatment has been compared with the QE measured before the treatment (Fig. 42). Some QE reduction is observed below ≈160 nm, most likely related to surface oxidation that can take place during the heating treatment in air. A different protocol with heat treatment in inert atmosphere is been considered in order to prevent oxidation. It will also require setup modifications.

The effective QE versus the number of spray shots has been measured (Fig. 43). The effective QE figure is saturated at 50 spray shots.

The effective QE in gases is a key parameter for the performance of gaseous Photon Detectors (PD). This was immediately recognized when the first gaseous PDs have been developed within the CERN-based technological collaboration RD26 [25, 26]. They where using CsI as photoconverter. The effective QE in gas has

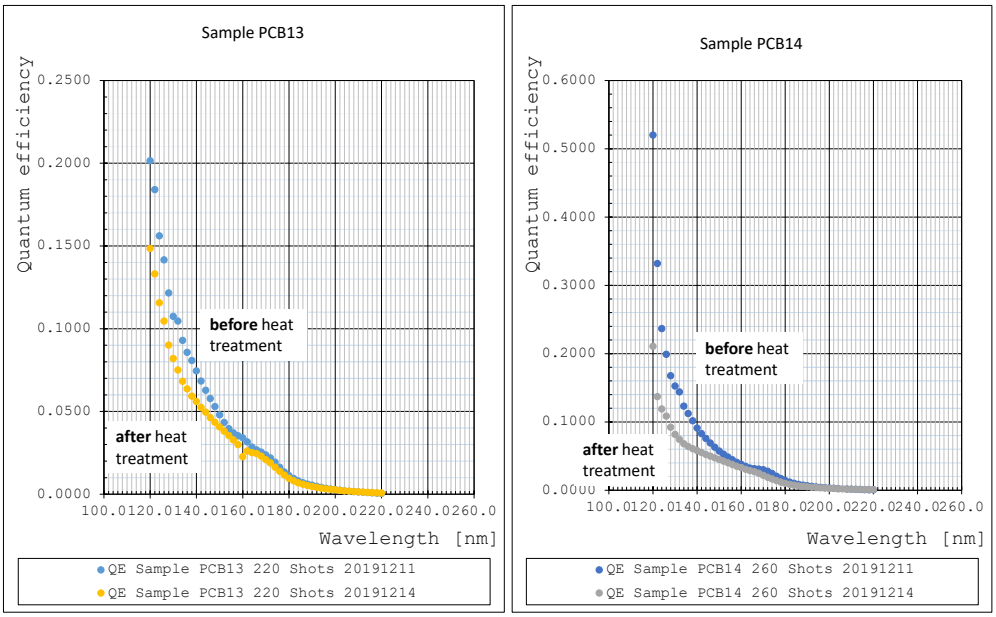

Figure 42: QE versus wavelength of two NHD-coated samples measured before and after the heat treatment.

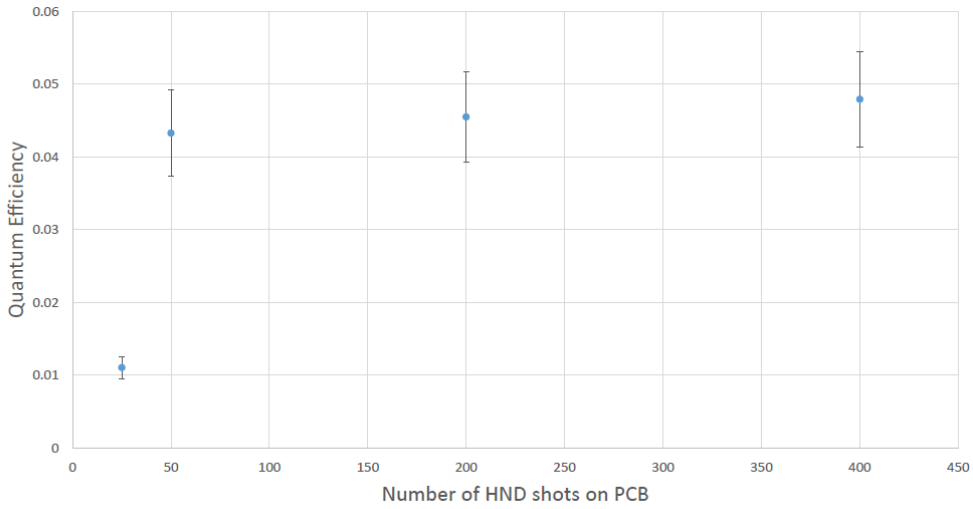

Figure 43: QE at 162 nm versus the number of HND spray shots applied to coat the sample.

been measured by several groups [27, 28, 29] and reproduced in simulation studies where the back scattering by the gas molecules is taken into account [30]. We have started exercises to measure the effective QE in gasses of interest when HND photocathodes are used. When the measurement campaign is completed, we will verify if the back scattering by the gas molecules is adequate to describe the effective QE also for the novel photoconverter. The first measurements are reported in Fig. 44. The observed evolution versus the electric field in front of the photocathode is similar to that observed for CsI.

The CERN EP-DT-DD GDD group is setting up a new facility known as ASSET[1], designed to be a pho-

[1]F. Brunbauer, private communication

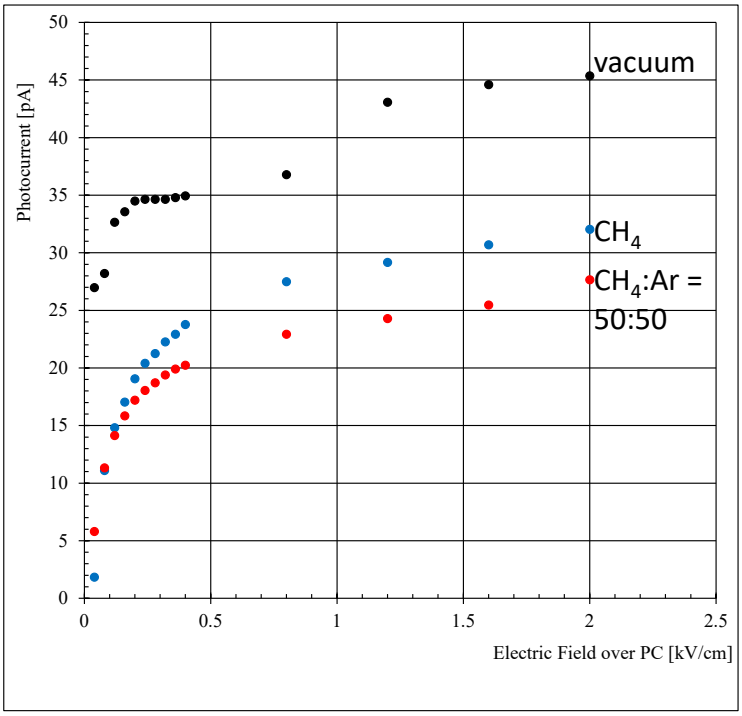

Figure 44: Normalized photocurrent measured at the photocathode illuminated with 162 nm light versus the electric field applied in front of the photocathode by HND powder. The light yield is normalized using light intensity measurements performed with a calibrated photodiode. A measurement in vacuum is also reported for comparison.

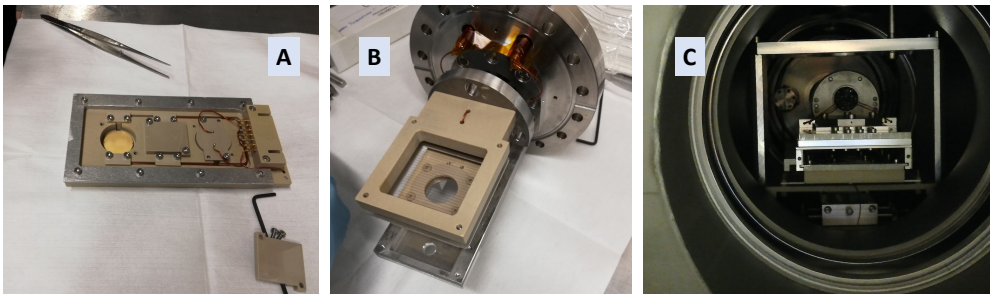

Figure 45: Preparation for the radiation hardness measurements of the HND photocathodes in the ASSET facility. (A) The support for our disc samples; (B) the support mounted together with the wire plane used in ASSET for QE measurements in reflection mode; (C) the support and the wire plane inserted in the ASSET setup.

tocathode characterisation device. The device is design to make possible QE measurements in reflection and transmission mode, and it will offer the possibility to perform ageing studies of photocathodes receiving controlled doses of ion bombardment. We have designed and built specific supports for our disk samples, which are compatible with ASSET (Fig. 45). One of the goals of the measurements at ASSET is to perform, in the next months, radiation hardness studies of the HND photocathodes.

In conclusion, relevant advancement has been registered in overcoming the low electrical rigidity of THGEM with HND coating, in measuring the effective QE obtained using THGEMs in different atmospheres and

starting systematic studies to optimize the parameters of the spray technique used for HND coating. The exercises reported above also suggest the next steps, which are presented in Sec. 3.1.4.2. These results fully match the planned activity. The preparation for the radiation hardness measurements is beyond the planning.

3.1.3 What was not achieved, why not and what will be done to correct?

3.1.3.1 MPGD sensors of single photons at INFN Trieste

The activity has partially deviated from the planning. The ongoing analysis of the test beam data and the further laboratory studies of the prototype with miniaturized pads, have made clear that the too high noise level of the present implementation prevents us from obtaining a complete characterization of the proposed detector architecture and accessing its intrinsic performance. Therefore, the activity planning has been readjusted giving priority to activities aimed to overcome the high noise feature, as discussed in detail in Sec. 3.1.2.1. The new activity planning has prevented from matching the **milestones for 2019**:
"September 2019: The completion of the laboratory characterization of the second version of the photon detector with miniaturized pad-size."

3.1.3.2 New Photocathode Materials development at INFN Trieste

The exploratory activity is progressing according to the planning. The **milestone for 2019**
"September 2019: The completion of the studies to understand the performance of THGEMs with ND coating, both in the hydrogenized and non-hydrogenized versions."
has been matched.

3.1.4 What is planned for the next funding cycle and beyond?

3.1.4.1 MPGD sensors of single photons at INFN Trieste

The construction of the second version of the prototype is foreseen for the year 2020, as well as the initial characterization studies.

The construction of a dedicated micromegas prototype for comparative studies of the current FE chip, namely APV25, and the newly considered one, namely VMM3, is scheduled in 2020 as well as the initial comparative exercises.

3.1.4.2 New Photocathode Materials development at INFN Trieste

The next activity steps are related to the results presented in Sec. 3.1.2.2 and represent the natural continuation of the on-going program.

The heat treatment, that allows recovering the required electrical rigidity of HND coated THGEMs, has been applied in air atmosphere. Some reduction of the QE is observed, most likely related to oxidation in air. The heat treatment protocol needs to be modified heating in inert atmosphere. Then, it will be verified if the effective QE is preserved.

The measurements to establish the effective QE of HND photocathodes will be completed.

The investigation of ND powder parameters influencing the QE performance will be continued.

First measurements of HND radiation hardness will be performed in the ASSET setup at CERN.



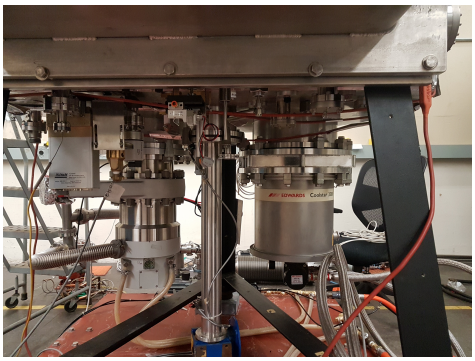

Figure 46: Left: Outside view of the evaporator with service racks. Middle: Inside view. Right: Bottom view.

3.2 Optical Elements - SBU

3.2.1 What was planned for this period?

3.2.1.1 Large mirrors development at Stony Brook

The installation of the electron-gun, ion-gun, and motor-rotated shaft was planned to be finalized in the last months.

3.2.1.2 New Radiator Studies at Stony Brook

It was planned and expected that students were familiarized with simulation software and to start designing models for simulating possible meta-materials.

3.2.2 What was achieved?

3.2.2.1 Large mirrors development at Stony Brook

The required equipment for upgrading the evaporator has been installed. Services that are needed to operate the vacuum generation and auxiliaries were installed. The installed equipment can be seen in Fig. 46. We are now verifying that the evaporator is in operational condition (pumping equipment, leak checking, etc.) and we are familiarizing ourselves with how to operate the equipment which will eventually lead to the commissioning of the upgraded device.
A mock-up device (Fig. 47) which mimics the mirror blank to be evaporated for a large scale mirror in SoLID has been constructed for installation in the evaporator. The mock-up device has a series of small surface devices (pillars) on which the `Al` and subsequent MgF_2 evaporation will be performed. The size of the pillars was chosen such that they will fit in the spectrum analyzer provided by the BNL group for analyzing the quality of the evaporation.

3.2.2.2 New Radiator Studies at Stony Brook

SBU students are in the process of modelling arrangements and geometries of materials that promise to be providing anisotropic refractive indices depending on the path of charged particles to be identified in collisions in an EIC.

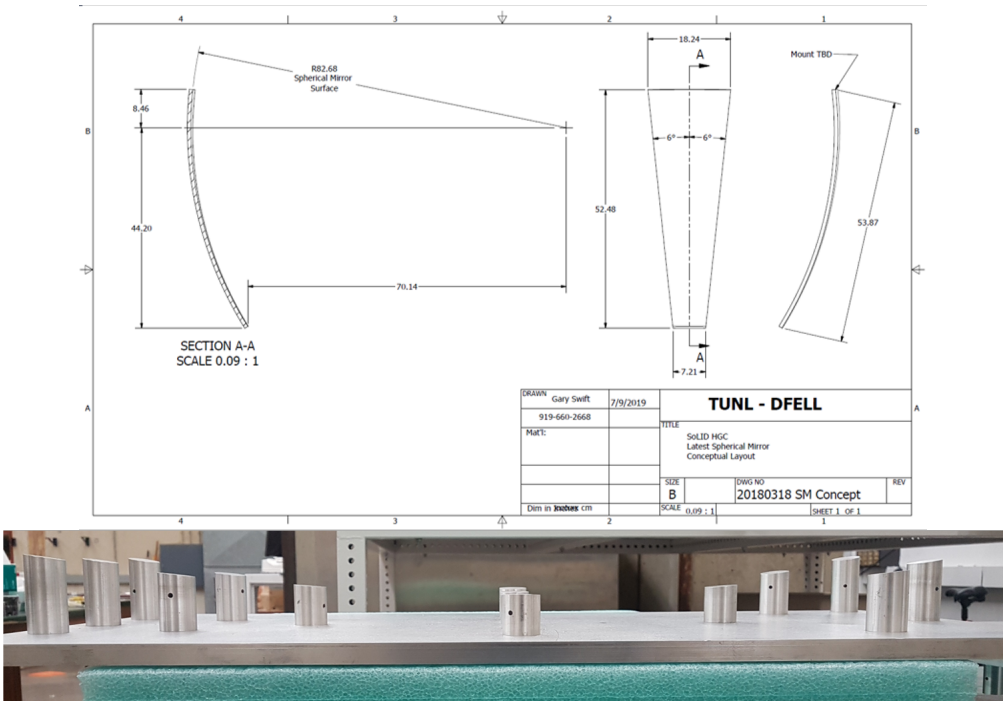

Figure 47: Sketch of a possible RICH mirror (SoLID) and mock-up device for mirror coating. The pillars' height and shape are following the curvature of the mirror and serve as samples which are removable and can be placed in a spectrum analyzer for verifying the reflectivity.

3.2.3 What was not achieved, why not and what will be done to correct?

3.2.3.1 Large mirrors development at Stony Brook

After finalizing the installation of the upgrade for the evaporator the commissioning of the device has yet to be performed. We are in the process of getting familiar with the operation of the equipment and we will then start with the commissioning and operation.
In the meantime we were practicing the evaporation with samples in a small scale evaporator with similar performance parameters provided by a local expert at SBU.

3.2.3.2 New Radiator Studies at Stony Brook

The consultation with experts in the field has not yet happened, mainly due to scheduling issues and unresponsiveness. The release of the software MIRaGE provided by Sandia Labs has not happened and the status is unknown. Responses to inquiries from our side were not answered but we are patiently awaiting a sign.
In the meantime, we are studying literature and working on an approach that might be promising.

3.2.4 What is planned for the next funding cycle and beyond?

3.2.4.1 Large mirrors development at SBU

The commissioning of the newly installed equipment is imminent. We are in the process of switching on the equipment while this report is being submitted. We are concurrently rehearsing the operation of evaporation

with a small scale device that is operated by the condensed matter group at SBU, by the expert who was crucial in acquiring the equipment that we purchased.
Our first attempt to evaporate will be in connection with a calibration unit for a TPC by means of a laser illumination device.

3.2.4.2 New Radiator Studies at Stony Brook

We are working on the development of a software framework that enables us to generate a feasible solution to the problem of the arrangement and dimensioning of materials for a medium to provide anisotropic indices of refraction. The framework will make use of neural networks [31] and requires a reasonable large training set that will come from FEM calculations with our acquired COMSOL software. The training set will be established with a limited set of FEM calculations by means of the T-matrix procedure [32].
Materials under consideration have to be investigated according to their composition as well to their geometric arrangement. Testing different materials under various configuration is a very time consuming endeavor. One can circumvent the tedious trial and error approach by simulating the response of single materials under different geometrical configurations with a countable series of simulations. When analyzing the response of that material to incident and scattered electromagnetic waves one can obtain a transition matrix that describes in a generic way the behavior of the material as a scattering object with multiple plane wave illuminations. The procedure is known as the T-matrix calculation via

$$\begin{pmatrix} \vec{a} \\ \vec{b} \end{pmatrix} = \mathbf{T} \begin{pmatrix} \vec{c} \\ \vec{d} \end{pmatrix}$$

Here $\vec{a}$ and $\vec{b}$ are concatenated vectors that contain the scattering coefficients of the outgoing wave and $\vec{c}$ and $\vec{d}$ are concatenated vectors containing the coefficients of the incident field and have to be calculated with FEM. The vectors will be used to determine $\mathbf{T}$ which is the T-matrix. It contains the entire near and far field information on how a specific object interacts with any illumination. It depends on the geometry and material composition of the structure in question.
Data-driven approaches based on deep-learning technology have been very successful in the field of nanophotonics by allowing efficient inverse design methods. A neural network can learn the correlation between material and geometry information by means of developing and training with a large data set. The training will lead to a repeated employment for designing photonic structures from given arbitrary optical properties. Various T-matrices obtained with the above mentioned procedure will serve as input for the data sets by providing the optical properties. Such design process will take only a fraction of time compared to conventional labor-intensive parameter optimization methods. Upon examination of the obtained optical properties we will simulate in detail such configuration and attempt to study the realization process for fabricating the device.

4 Critical Issues

4.1 Brookhaven National Lab

Though we have settled on what we believe is an optimal zigzag pattern for the TPC, this decision is based on data gathered from planar detectors with minimal transverse diffusion. To fully optimize the pattern, it will be critical to iterate on the design based on the results from the measurements with the new readout board currently being produced at CERN. We would therefore need additional funding from eRD6 to continue this effort in order to optimize a TPC readout specifically for EIC applications.

4.2 Florida Tech

The departure of our post-doc Aiwu Zhang back in December 2016 without replacement has slowed down progress ever since. Also, Matt Bomberger, our graduate students working on the forward tracker, had to take a leave of absence in December 2019 that is expected to last at least until summer 2020. We have found a temporary replacement for next semester, graduate student Brendan Steffens, but the required on-the-job training will slow down progress.

4.3 INFN Trieste

No technical critical issue is expected for the completion of the planed 2020 activity.

4.4 Stony Brook University

Despite protracted activities in producing a workable sample for new radiator materials, this was nevertheless expected and we therefore do not have any critical issue.

4.5 Temple University

None.

4.6 University of Virginia

No critical issues.

5 Additional information

5.1 Brookhaven National Lab

As mentioned in prior progress reports, the work on optimizing the geometrical parameters that define the shape of the zigzag charge collecting anodes is primarily funded by a separate BNL LDRD program. We traditionally mention the results from this R&D program in this report because of their direct relevance for our eRD6 activities. However, it must be emphasized that the LDRD program is focused on optimizing zigzag patterns for planar detectors, not for a TPC. We would therefore need additional support from eRD6 to continue this effort.

6 Manpower

6.1 Brookhaven National Lab

Our total manpower effort on MPGDs for EIC, which includes eRD6 as well as other activities, is listed below. All scientific and engineering manpower is being supported by internal BNL funds. Funds are requested from eRD6 for technical support.

6.1.1 Total manpower effort for MPGD R&D

- 2 Senior Scientists: Martin Purschke (0.2 FTE), Craig Woody (0.2 FTE)
- 1 Scientist: Alexander Kiselev (0.4 FTE)
- 1 Physics Associate: Bob Azmoun (0.8 FTE)
- 1 Electronics Engineer: John Kuczewski (0.1 FTE)
- 1 Technician: Bill Lenz (0.5 FTE).

6.1.2 Portion of the effort listed above being devoted to eRD6 activities

- 2 Senior Scientists: Martin Purschke (0.1 FTE), Craig Woody (0.1 FTE)
- 1 Scientist: Alexander Kiselev (0.2 FTE)
- 1 Physics Associate: Bob Azmoun (0.2 FTE)
- 1 Electronics Engineer: John Kuczewski (0.1 FTE)
- 1 Technician: Bill Lenz (0.3 FTE).

6.2 Florida Tech

- Marcus Hohlmann, Professor, 0.25 FTE, not funded under this R&D program.
- Matthew Bomberger, physics graduate student (M.S.), funded with $8.2k stipend in fall 2019 by this R&D program.
- Jerry Collins, physics graduate student (M.S.), funded with $8.2k stipend in fall 2019 by this R&D program.
- Michael Werbiskis, physics undergraduate student, not funded.

6.3 INFN Trieste

From INFN Trieste:

- C. Chatterjee (Trieste University and INFN, PhD student)
- D. D'Ago (Trieste University and INFN, PhD student)
- S. Dalla Torre (INFN, Staff)
- S. Dasgupta (INFN, postdoc)
- S. Levorato (INFN, staff)
- F. Tessarotto (INFN, Staff)
- Triloki (ICTP and INFN, fellowship)

The contribution of technical personnel from INFN-Trieste is also foreseen according to needs.

From INFN BARI:

- Grazia Cicala (CNR staff and INFN)
- T. Ligonzo (Bari University and INFN, professor)
- Antonio Valentini (Bari University and INFN, professor)

Globally, the dedicated manpower is equivalent to 3 FTE.

6.4 Stony Brook University

- K. Dehmelt, Research Scientist, 0.3 FTE
- T. K. Hemmick, Professor, 0.1 FTE
- P. Garg, Postdoc, 0.1 FTE
- C. Perez Lara, Postdoc, 0.1 FTE
- A. Kulkarni, Grad student, 0.75 FTE
- V. Zakharov, Grad student, 0.5 FTE

None of the personnel is funded under this R&D program.

6.5 Temple University

- B. Surrow, Professor, 0.1 FTE
- M. Posik, Assistant Research Professor, 0.2 FTE
- A. Quintero, Post-doc, 0.2 FTE
- J. Nam and N. Lukow, graduate student, 0.1 FTE

6.6 University of Virginia

None of the labor at UVa is funded by EIC R&D. The workforce is listed below:

- Nilanga Liyanage; Professor; 0.1 FTE
- Kondo Gnanvo; Senior Research Scientist; 0.3 FTE
- Minh Dao; Junior Student; 0.2 FTE
- Huong Nguyen; Senior Research Scientist; 0.1 FTE
- John Boyd; Grad Student; 0.1 FTE

7 List of all EIC publications from the eRD6 Consortium

BNL publications:

[1] B. Azmoun et al. "Results From a Prototype Combination TPC Cherenkov Detector With GEM Readout". In: *IEEE Transactions on Nuclear Science* 66.8 (Aug. 2019), pp. 1984–1992. ISSN: 1558-1578. DOI: 10.1109/TNS.2019.2928269.

[2] Maxence Vandenbroucke et al. "A Study of "Zigzag" Strip Readout for Micromegas Detectors". In: Nov. 2018, pp. 1–4. DOI: 10.1109/NSSMIC.2018.8824702.

[3] B. Azmoun et al. "Design Studies for a TPC Readout Plane Using Zigzag Patterns with Multistage GEM Detectors". In: *IEEE Transactions on Nuclear Science* (July 2018), pp. 1–1. ISSN: 0018-9499. DOI: 10.1109/TNS.2018.2846403.

[4] B. Azmoun et al. "A Study of a Mini-Drift GEM Tracking Detector". In: *IEEE Transactions on Nuclear Science* 63.3 (June 2016), pp. 1768–1776. ISSN: 0018-9499. DOI: 10.1109/TNS.2016.2550503.

[5] Craig Woody et al. "A Prototype Combination TPC Cherenkov Detector with GEM Readout for Tracking and Particle Identification and its Potential Use at an Electron Ion Collider". In: 2015. arXiv: 1512.05309 [physics.ins-det]. URL: https://inspirehep.net/record/1409973/files/arXiv:1512.05309.pdf.

[6] B. Azmoun et al. "Initial studies of a short drift GEM tracking detector". In: *2014 IEEE Nuclear Science Symposium and Medical Imaging Conference (NSS/MIC)*. Nov. 2014, pp. 1–2. DOI: 10.1109/NSSMIC.2014.7431059.

[7] M. L. Purschke et al. "Test beam study of a short drift GEM tracking detector". In: *2013 IEEE Nuclear Science Symposium and Medical Imaging Conference (2013 NSS/MIC)*. Oct. 2013, pp. 1–4. DOI: 10.1109/NSSMIC.2013.6829463.

Florida Tech publications:

[1] Marcus Hohlmann et al. "Low-mass GEM detector with radial zigzag readout strips for forward tracking at the EIC". In: *2017 IEEE Nuclear Science Symposium and Medical Imaging Conference (NSS/MIC 2017) Atlanta, Georgia, USA, October 21-28, 2017*. 2017. arXiv: 1711.05333 [physics.ins-det]. URL: http://inspirehep.net/record/1636290/files/arXiv:1711.05333.pdf.

[2] Aiwu Zhang et al. "A GEM readout with radial zigzag strips and linear charge-sharing response". In: *Nucl. Instrum. Meth.* A887 (2018), pp. 184–192. arXiv: 1708.07931 [physics.ins-det].

[3] Aiwu Zhang and Marcus Hohlmann. "Accuracy of the geometric-mean method for determining spatial resolutions of tracking detectors in the presence of multiple Coulomb scattering". In: *JINST* 11.06 (2016), P06012. DOI: 10.1088/1748-0221/11/06/P06012. arXiv: 1604.06130 [physics.data-an].

[4] Aiwu Zhang et al. "R&D on GEM detectors for forward tracking at a future Electron-Ion Collider". In: *Proceedings, 2015 IEEE Nuclear Science Symposium and Medical Imaging Conference (NSS/MIC 2015): San Diego, California, United States*. 2016, p. 7581965. DOI: 10.1109/NSSMIC.2015.7581965. arXiv: 1511.07913 [physics.ins-det]. URL: http://inspirehep.net/record/1406551/files/arXiv:1511.07913.pdf.

[5] Aiwu Zhang et al. "Performance of a Large-area GEM Detector Read Out with Wide Radial Zigzag Strips". In: *Nucl. Instrum. Meth.* A811 (2016), pp. 30–41. DOI: 10.1016/j.nima.2015.11.157. arXiv: 1508.07046 [physics.ins-det].

INFN publications:

[1] J. Agarwala et al. "The MPGD-based photon detectors for the upgrade of COMPASS RICH-1 and beyond". In: *Nuclear Instruments and Methods in Physics Research Section A: Accelerators, Spectrometers, Detectors and Associated Equipment* (2018). ISSN: 0168-9002. DOI: https://doi.org/10.1016/j.nima.2018.10.092. URL: http://www.sciencedirect.com/science/article/pii/S0168900218314062.

[2] J. Agarwala et al. "Study of MicroPattern Gaseous detectors with novel nanodiamond based photocathodes for single photon detection in EIC RICH". In: *Nuclear Instruments and Methods in Physics Research Section A: Accelerators, Spectrometers, Detectors and Associated Equipment* (2019). ISSN: 0168-9002. DOI: https://doi.org/10.1016/j.nima.2019.03.022. URL: http://www.sciencedirect.com/science/article/pii/S0168900219303213.

[3] J. Agarwala et al. "Optimized MPGD-based Photon Detectors for high momentum particle identification at the Electron-Ion Collider". In: *Nuclear Instruments and Methods in Physics Research Section A: Accelerators, Spectrometers, Detectors and Associated Equipment* 936 (2019). Frontier Detectors for Frontier Physics: 14th Pisa Meeting on Advanced Detectors, pp. 565–567. ISSN: 0168-9002. DOI: https://doi.org/10.1016/j.nima.2018.10.185. URL: http://www.sciencedirect.com/science/article/pii/S0168900218314992.

[4] J. Agarwala et al. *A modular mini-pad photon detector prototype for RICH application at the Electron Ion Collider*. 2019. arXiv: 1908.05052 [physics.ins-det].

[5] C. Chatterjee et al. *Nanodiamond photocathodes for MPGD-based single photon detectors at future EIC*. 2019. arXiv: 1908.05058 [physics.ins-det].

SBU publications:

[1] M. Blatnik et al. "Performance of a Quintuple-GEM Based RICH Detector Prototype". In: *IEEE Trans. Nucl. Sci.* 62.6 (2015), pp. 3256–3264. DOI: 10.1109/TNS.2015.2487999. arXiv: 1501.03530 [physics.ins-det].

TU publications:

[1] M. Posik and B. Surrow. "Construction of a Triple-GEM Detector Using Commercially Manufactured Large GEM Foils". In: 2018. arXiv: 1806.01892 [physics.ins-det].

[2] M. Posik and B. Surrow. "Construction of Triple-GEM Detectors Using Commercially Manufactured Large GEM Foils". In: *Proceedings, 2016 IEEE Nuclear Science Symposium and Medical Imaging Conference: NSS/MIC 2016: Strasbourg, France*. 2016, p. 8069743. DOI: 10.1109/NSSMIC.2016.8069743. arXiv: 1612.03776 [physics.ins-det].

[3] M. Posik and B. Surrow. "Optical and electrical performance of commercially manufactured large GEM foils". In: *Nucl. Instrum. Meth.* A802 (2015), pp. 10–15. DOI: 10.1016/j.nima.2015.08.048. arXiv: 1506.03652 [physics.ins-det].

[4] M. Posik and B. Surrow. "R&D of commercially manufactured large GEM foils". In: *Proceedings, 2015 IEEE Nuclear Science Symposium and Medical Imaging Conference (NSS/MIC 2015): San Diego, California, United States*. 2016, p. 7581802. DOI: 10.1109/NSSMIC.2015.7581802. arXiv: 1511.08693 [physics.ins-det].

[5] M. Posik and B. Surrow. "Research and Development of Commercially Manufactured Large GEM Foils". In: *Proceedings, 21st Symposium on Room-Temperature Semiconductor X-ray and Gamma-ray Detectors (RTSD 2014): Seattle, WA, USA, November 8-15, 2014*. 2016, p. 7431060. DOI: 10.1109/NSSMIC.2014.7431060. arXiv: 1411.7243 [physics.ins-det].

UVa publications:

[1] Kondo Gnanvo et al. "Large Size GEM for Super Bigbite Spectrometer (SBS) Polarimeter for Hall A 12 GeV program at JLab". In: *Nucl. Instrum. Meth.* A782 (2015), pp. 77–86. DOI: 10.1016/j.nima.2015.02.017. arXiv: 1409.5393 [physics.ins-det].

[2] Kondo Gnanvo et al. "Performance in test beam of a large-area and light-weight GEM detector with 2D stereo-angle (UV) strip readout". In: *Nucl. Instrum. Meth.* A808 (2016), pp. 83–92. DOI: 10.1016/j.nima.2015.11.071. arXiv: 1509.03875 [physics.ins-det].

Yale publications:

[1] S. Aiola et al. "Combination of two Gas Electron Multipliers and a Micromegas as gain elements for a time projection chamber". In: *Nucl. Instrum. Meth.* A834 (2016), pp. 149–157. DOI: 10.1016/j.nima.2016.08.007. arXiv: 1603.08473 [physics.ins-det].

References

[1] B. Azmoun et al. "A Study of a Mini-Drift GEM Tracking Detector". In: *IEEE Transactions on Nuclear Science* 63.3 (June 2016), pp. 1768–1776. ISSN: 0018-9499. DOI: 10.1109/TNS.2016.2550503.

[2] B. Azmoun et al. "Results From a Prototype Combination TPC Cherenkov Detector With GEM Readout". In: *IEEE Transactions on Nuclear Science* 66.8 (Aug. 2019), pp. 1984–1992. ISSN: 1558-1578. DOI: 10.1109/TNS.2019.2928269.

[3] B. Azmoun et al. "Design Studies for a TPC Readout Plane Using Zigzag Patterns with Multistage GEM Detectors". In: *IEEE Transactions on Nuclear Science* (July 2018), pp. 1–1. ISSN: 0018-9499. DOI: 10.1109/TNS.2018.2846403.

[4] B. Azmoun et al. "Design Studies of High Resolution Readout Planes using Zigzags with GEM Detectors". In: *IEEE Transactions on Nuclear Science* (2020). Submitted to IEEE Transactions on Nuclear Science.

[5] Aiwu Zhang et al. "Performance of a Large-area GEM Detector Read Out with Wide Radial Zigzag Strips". In: *Nucl. Instrum. Meth.* A811 (2016), pp. 30–41. DOI: 10.1016/j.nima.2015.11.157. arXiv: 1508.07046 [physics.ins-det].

[6] Aiwu Zhang et al. "A GEM readout with radial zigzag strips and linear charge-sharing response". In: *Nucl. Instrum. Meth.* A887 (2018), pp. 184–192. arXiv: 1708.07931 [physics.ins-det].

[7] Marcus Hohlmann et al. "Low-mass GEM detector with radial zigzag readout strips for forward tracking at the EIC". In: *2017 IEEE Nuclear Science Symposium and Medical Imaging Conference (NSS/MIC 2017) Atlanta, Georgia, USA, October 21-28, 2017*. 2017. arXiv: 1711.05333 [physics.ins-det]. URL: http://inspirehep.net/record/1636290/files/arXiv:1711.05333.pdf.

[8] J. Agarwala et al. "The MPGD-based photon detectors for the upgrade of COMPASS RICH-1 and beyond". In: *Nuclear Instruments and Methods in Physics Research Section A: Accelerators, Spectrometers, Detectors and Associated Equipment* (2018). ISSN: 0168-9002. DOI: https://doi.org/10.1016/j.nima.2018.10.092. URL: http://www.sciencedirect.com/science/article/pii/S0168900218314062.

[9] E. Albrecht et al. "Status and characterisation of COMPASS RICH-1". In: *Nuclear Instruments and Methods in Physics Research Section A: Accelerators, Spectrometers, Detectors and Associated Equipment* 553.1 (2005). Proceedings of the fifth International Workshop on Ring Imaging Detectors, pp. 215–219. ISSN: 0168-9002. DOI: https://doi.org/10.1016/j.nima.2005.08.036. URL: http://www.sciencedirect.com/science/article/pii/S0168900205016001.

[10] P. Abbon et al. "Read-out electronics for fast photon detection with COMPASS RICH-1". In: *Nuclear Instruments and Methods in Physics Research Section A: Accelerators, Spectrometers, Detectors and Associated Equipment* 587.2 (2008), pp. 371–387. ISSN: 0168-9002. DOI: https://doi.org/10.1016/j.nima.2007.12.026. URL: http://www.sciencedirect.com/science/article/pii/S0168900207024576.

[11] P. Abbon et al. "Design and construction of the fast photon detection system for COMPASS RICH-1". In: *Nuclear Instruments and Methods in Physics Research Section A: Accelerators, Spectrometers, Detectors and Associated Equipment* 616.1 (2010), pp. 21–37. ISSN: 0168-9002. DOI: https://doi.org/10.1016/j.nima.2010.02.069. URL: http://www.sciencedirect.com/science/article/pii/S0168900210002676.

[12] P. Abbon et al. "Particle identification with COMPASS RICH-1". In: *Nuclear Instruments and Methods in Physics Research Section A: Accelerators, Spectrometers, Detectors and Associated Equipment* 631.1 (2011), pp. 26–39. ISSN: 0168-9002. DOI: https://doi.org/10.1016/j.nima.2010.11.106. URL: http://www.sciencedirect.com/science/article/pii/S0168900210026422.

[13] P. Abbon et al. "The COMPASS experiment at CERN". In: *Nuclear Instruments and Methods in Physics Research Section A: Accelerators, Spectrometers, Detectors and Associated Equipment* 577.3 (2007), pp. 455–518. ISSN: 0168-9002. DOI: https://doi.org/10.1016/j.nima.2007.03.026. URL: http://www.sciencedirect.com/science/article/pii/S0168900207005001.

[14] P. Abbon et al. "The COMPASS setup for physics with hadron beams". In: *Nuclear Instruments and Methods in Physics Research Section A: Accelerators, Spectrometers, Detectors and Associated Equipment* 779.Supplement C (2015), pp. 69–115. ISSN: 0168-9002. DOI: https://doi.org/10.1016/j.nima.2015.01.035. URL: http://www.sciencedirect.com/science/article/pii/S0168900215000662.

[15] Luciano Velardi, Antonio Valentini, and Grazia Cicala. "UV photocathodes based on nanodiamond particles: Effect of carbon hybridization on the efficiency". In: *Diamond and Related Materials* 76.Supplement C (2017), pp. 1–8. ISSN: 0925-9635. DOI: https://doi.org/10.1016/j.diamond.2017.03.017. URL: http://www.sciencedirect.com/science/article/pii/S0925963516306999.

[16] Kondo Gnanvo et al. "Performance in test beam of a large-area and light-weight GEM detector with 2D stereo-angle (UV) strip readout". In: *Nucl. Instrum. Meth.* A808 (2016), pp. 83–92. DOI: 10.1016/j.nima.2015.11.071. arXiv: 1509.03875 [physics.ins-det].

[17] M. Poli Lener. "The Micro-RWELL". In: *CepC Workshop* (2018).

[18] P. Abbon et al. "A new analogue sampling readout system for the COMPASS RICH-1 detector". In: *Nuclear Instruments and Methods in Physics Research Section A: Accelerators, Spectrometers, Detectors and Associated Equipment* 589.3 (2008), pp. 362–369. ISSN: 0168-9002. DOI: https://doi.org/10.1016/j.nima.2008.02.077. URL: http://www.sciencedirect.com/science/article/pii/S0168900208003148.

[19] G. De Geronimo; J. Fried; S. Li; J. Metcalfe; N. Nambiar; E. Vernon; V. Polychronakos. "VMM1—An ASIC for Micropattern Detectors". In: *IEEE Transactions on Nuclear Science* 60.3 (2013), pp. 2314–2321. DOI: 10.1109/TNS.2013.2258683. URL: https://ieeexplore-ieee-org.ezproxy.cern.ch/document/6518121/.

[20] *Performance of the First Version of VMM Front-End ASIC with Resistive Micromegas Detectors*. Tech. rep. ATL-UPGRADE-PUB-2014-001. Geneva: CERN, Sept. 2014. URL: https://cds.cern.ch/record/1753328.

[21] Georgios Iakovidis. "Research and Development in Micromegas Detector for the ATLAS Upgrade". Presented 13 Oct 2014. Oct. 2014. URL: https://cds.cern.ch/record/1955475.

[22] Georgios Iakovidis. *VMM3, an ASIC for Micropattern Detectors*. Tech. rep. ATL-MUON-PROC-2018-003. Geneva: CERN, Mar. 2018. URL: http://cds.cern.ch/record/2309951.

[23] M.J. French et al. "Design and results from the APV25, a deep sub-micron CMOS front-end chip for the CMS tracker". In: *Nuclear Instruments and Methods in Physics Research Section A: Accelerators, Spectrometers, Detectors and Associated Equipment* 466.2 (2001). 4th Int. Symp. on Development and Application of Semiconductor Tracking Detectors, pp. 359–365. ISSN: 0168-9002. DOI: https://doi.org/10.1016/S0168-9002(01)00589-7. URL: http://www.sciencedirect.com/science/article/pii/S0168900201005897.

[24] A Valentini, E Nappi, and M.A Nitti. "Influence of the substrate reflectance on the quantum efficiency of thin CsI photocathodes". In: *Nuclear Instruments and Methods in Physics Research Section A: Accelerators, Spectrometers, Detectors and Associated Equipment* 482.1 (2002), pp. 238–243. ISSN: 0168-9002. DOI: https://doi.org/10.1016/S0168-9002(01)01678-3. URL: http://www.sciencedirect.com/science/article/pii/S0168900201016783.

[25] *Status report from the CsI-Rich Collaboration: R&D for the development of a large area advanced fast rich detector for particle identification at the LHC operated with heavy ions: RD-26*. Tech. rep. CERN-DRDC-93-36. DRDC-Status-report-RD-26. Geneva: CERN, 1993. URL: http://cds.cern.ch/record/291164.

[26] A Di Mauro, L Galantucci, and A Grimaldi. *Status report of the CSI-RICH Collaboration 1994: development of a large area advanced fast RICHC detector for particle identification at the LHC operated with heavy ions*. Tech. rep. CERN-DRDC-94-49. DRDC-RD-26. Geneva: CERN, 1994. URL: http://cds.cern.ch/record/294148.

[27] A. Breskin et al. "Field-dependent photoelectron extraction from CsI in different gases". In: *Nuclear Instruments and Methods in Physics Research Section A: Accelerators, Spectrometers, Detectors and Associated Equipment* 367.1 (1995). Proceedings of the 7th International Wire Chamber Conference, pp. 342–346. ISSN: 0168-9002. DOI: https://doi.org/10.1016/0168-9002(95)00639-7. URL: http://www.sciencedirect.com/science/article/pii/0168900295006397.

[28] M. Alexeev et al. "Micropattern gaseous photon detectors for Cherenkov imaging counters". In: *Nuclear Instruments and Methods in Physics Research Section A: Accelerators, Spectrometers, Detectors and Associated Equipment* 623.1 (2010). 1st International Conference on Technology and Instrumentation in Particle Physics, pp. 129–131. ISSN: 0168-9002. DOI: https://doi.org/10.1016/j.nima.2010.02.171. URL: http://www.sciencedirect.com/science/article/pii/S0168900210004389.

[29] C D R Azevedo et al. "Towards THGEM UV-photon detectors for RICH: on single-photon detection efficiency in Ne/CH4and Ne/CF4". In: *Journal of Instrumentation* 5.01 (Jan. 2010), P01002–P01002. DOI: 10.1088/1748-0221/5/01/p01002. URL: https://doi.org/10.1088%2F1748-0221%2F5%2F01%2Fp01002.

[30] J Escada et al. "Measurements of photoelectron extraction efficiency from CsI into mixtures of Ne with CH4, CF4, CO2and N2". In: *Journal of Instrumentation* 4.11 (Nov. 2009), P11025–P11025. DOI: 10.1088/1748-0221/4/11/p11025. URL: https://doi.org/10.1088%2F1748-0221%2F4%2F11%2Fp11025.

[31] Itzik Malkiel et al. "Plasmonic nanostructure design and characterization via Deep Learning". In: *Light: Science & Applications* 7 (Dec. 2018). DOI: 10.1038/s41377-018-0060-7.

[32] L. Tsang, J. A. Kong, and K.-H. Ding. *Scattering of Electromagnetic Waves, Theories and Applications*. July 2000, p. 445.